

Chemical Recycling of Poly(ethylene terephthalate): Effects of Mechanical Stress and Radiation Damage on Hydrolysis

by
Tongjie Zhang

A Thesis
Submitted to the Faculty
of the
WORCESTER POLYTECHNIC INSTITUTE
In partial fulfillment of the requirements for the
Degree of Master of Science

In
Chemical Engineering

April 2020

APPROVED:

Professor Michael T. Timko, Thesis Advisor

Professor Andrew R. Teixeira, Thesis Committee Member

Professor William M. Clark, Thesis Committee Member

Professor Nima Rahbar, Thesis Committee Member

Abstract

Finding an effective recycling process for oceanic plastic waste is increasingly important to address environmental pollution. Plastic waste is a bountiful and sustainable resource for energy production and chemical recycling. Polyethylene terephthalate (PET), one of the most common commercialized polymers, is promising to be recycled by hydrolysis. The objective of this work was to study the effects of mechanical stress and radiation damage on PET structure and hydrolysis reactivity. Ball-milling and photo-damaging pretreatments were carried out to imitate the environmental degradation in the ocean environment. An evident decrease in crystallinity with increasing ball-milling time was observed. This decrease in crystallinity caused by fractures of chemical bonds induced by photoaging and ball-milling treatments were investigated. PET was hydrolyzed into ethylene glycol (EG) and terephthalic acid (TPA) at 200°C in tube hydrolysis reactors without catalysts. EG and TPA were recovered after PET depolymerization. Thermogravimetric analysis and Fourier-transform infrared spectroscopy indicated that the recovered TPA was purified. Qualitative and quantitative analysis of TPA and EG were performed by using UV-Visible spectrophotometer and High-Performance Liquid Chromatograph (HPLC) separately. At 200 °C, the conversion rate of fresh and ball-milled PET samples was improved from 16-18% with a one-hour reaction time compared to 87-91% with a two-hour reaction time. This depolymerization behavior supported that the conversion rate of PET was increased with increasing reaction time at the same temperature. The experiment results, however, showed PET conversion, TPA yield, and EG yield did not improve after ball-milling and photo-damaging treatment. After retention time of 1 hour, PET conversions, yields of TPA, yields of EG of various PET samples were $16.5 \pm 1.5\%$, $11.5 \pm 1.5\%$ and $0.70 \pm 0.20\%$, respectively. Mechanical treatment and radiation damage did not affect PET reactivity significantly in this experiment. Two main

reasons were discussed to explain this result. The effect of radiation damage and mechanical stress was obscured by the more dominant reaction condition, temperature. The pretreatments in this experiment were not strong enough to affect PET reactivity. Based on the current results, recommendations for the hydrolysis temperature, potential catalysts, and more robust pretreatment methods were provided for further outlook of studying environmental effects on PET hydrolysis.

Acknowledgments

I would like to thank Worcester Polytechnic Institute and the Chemical Engineering Department first, which provides me with the opportunity to make progress on my research.

I would like to acknowledge Professor Michael T. Timko for his support, teaching, and suggestions through my master's study. I thrive on mastering difficulties through his education, which enables me to lay a foundation on thermodynamics and molecular interactions. He gave me lots of valuable advice on research communication skills and encouraged me to find the entailed information from my discoveries. Most importantly, he shaped me to be a budding engineer who is focusing on finding the backend mechanisms.

I would like to thank Professor Geoffrey Tompsett. He guided me on conducting research. He helped me build my reaction system and taught me a lot in characterization methods.

I would also like to acknowledge my committee member: Professor Andrew R. Teixeira, Professor William R. Clark, and Professor Nima Rahbar. They gave me constructive advice on my thesis and academic writing.

I appreciate all my groupmates in Prof. Timko's lab and Prof. Teixeira's lab. I would also like to express my thanks to Dr. Azadeh Zaker and Dr. Feng Cheng. They gave me lots of instructions on instrumental analysis, and help me with applying thermodynamics and hydrothermal liquefaction methods on my research. I would like to thank my coworkers, Ziyang Zhang, Cameron David Armstrong, and Joseph O. Heng, for their help in my coursework and research. I would like to thank Elizabeth Belden and Douglas Phillip Theberge for the revision and advice on my research.

I also appreciate all the technical help from Douglas White and Thomas Partington. Thanks to Leslie Brodeur and Royal Tiffany for their supports of administrative sides.

I am deeply grateful to Huan Chen at Florida State University. He helped me perform the radiation damage experiments of PET samples. He also gave me help and suggestions for my experimental methods.

Again, I would like to thank the supports, assistance, and encouragement from my family and friends through my master's.

Last but not least, I would like to thank all the people and communities making sure we have the essentials to survive on and even risking their health. They are the loveliest persons taking us through this crisis.

Table of contents

Abstract	II
Acknowledgments.....	IV
Table of contents.....	VI
List of Tables	X
List of Figures.....	XII
Part 1 Introduction	1
Part 2 Background.....	6
2.1 Chemical recycling of Poly (ethylene terephthalate)	6
2.1.1 Methods for recovering TPA and EG from PET	6
2.1.2 Chemical recycling of PET by hydrolysis	7
2.2 Depolymerization of PET by using water at higher temperatures	8
2.2.1 Depolymerization behavior of neutral hydrolytic depolymerization of PET	8
2.2.2 Reaction kinetics of PET hydrolysis	9
2.3 Structural features of PET and its measurement methods.....	10
2.3.1 Crystallinity of PET.....	10
2.3.2 XRD measurement of PET crystallinity.....	11
2.3.3 Crystallization Behavior of PET and Mechanical Milling	12
2.3.4 Photodegradation induced by ultraviolet light.....	13

2.4 Characterizations and measurements of PET hydrolyzed products	13
2.4.1 TPA recovery	13
2.4.2 Characterization and measurements of TPA	14
Part 3 Experiments	15
3.1 Materials	15
3.2 Pretreatment of PET samples and characterizations	16
3.2.1 Mechanical milling of PET	16
3.2.2 X-ray diffraction (XRD)	17
3.2.3 Radiation damage	17
3.2.4 Chemical-bond analysis: Raman microscopy and FT-IR	18
3.3 Tube hydrolysis reactor experiment	19
3.3.1 Reactor constructions and safety considerations	19
3.3.2 Hydrothermal experiment of PET in the tubular reactors	21
3.3.3 Recovery procedures of end products	22
3.4 Analysis of end products	24
3.4.1 Analysis of UV-Visible spectrophotometer	25
3.4.2 FT-IR analysis	25
3.4.3 TGA/ DTA analysis	25
3.4.4 HPLC analysis	26
Part 4 Results and Discussion	27

4.1 Structural features of pretreated PET	28
4.1.1. XRD data and crystallinity	28
4.1.2 Chemical-bond analysis: Raman microscopy and FT-IR.....	32
4.1.3 SEM and PET morphology.....	34
4.2.1 Characterization of Terephthalic Acid	35
4.2.1.1 TGA/DTG analysis of TPA.....	35
4.2.1.2 FT-IR analysis of TPA	37
4.2.1.3 Quantitative analysis by UV-visible spectrophotometer	38
4.2.2 Characterization of Ethylene Glycol	39
4.3 Kinetic Analysis of PET hydrolysis	40
4.3.1 Condition selection based on PET conversions.....	40
4.3.2 The activation energy of PET hydrolysis	41
4.4 Conversion rates and product yields of PET hydrolysis	43
4.4.1 Evaluation of PET reactivity after ball-milling treatment	44
4.4.2 Comparisons of PET and cellulose reactivity after ball-milling	46
4.4.3 Evaluation of PET reactivity after photoaging treatment.....	47
Part 5 Conclusions	49
Part 6 Future Outlooks	50
6.1 Recommendations for improved analytical techniques	50
6.1.1 Analysis of chemical modifications induced by UV laser	50

6.1.2 Surface chemistry study of PET samples	50
6.1.3 Molecular weight evaluations.....	51
6.2 Directions for PET hydrolysis study	51
6.2.1 Improved experimental procedures for the future study	51
6.2.2 Future work for improving ethylene glycol yield.....	52
Part 7 References	53
Appendix.....	61
A Parameters of Tube Hydrolysis Reactor Design	61
B Recent calibration for ethylene glycol (EG).....	63
C Recent calibration for terephthalic acid (TPA).....	64
D Raw data of PET conversion rates and yields of products	66
E XRD peak fitting.....	68
F FT-IR spectra of recovered TPA.....	69

List of Tables

TABLE 1 KINETICS OF PET HYDROLYSIS AT DIFFERENT TEMPERATURES WITH THE SAME RETENTION TIME	41
TABLE 2 PARAMETERS FOR THE DESIGN, SAFETY AND CONSTRUCTION OF TUBE HYDROLYSIS REACTORS ADAPTED FROM "TUBE FITTING PERFORMANCE PRODUCT TEST REPORTS," 2018 [65].	61
TABLE 3 TUBE PRESSURE RATINGS (A) AND STEAM TABLE DATA (B) FOR REACTOR DESIGN.	61
TABLE 4 RAW DATA OF ETHYLENE GLYCOL STANDARDS	63
TABLE 5 RAW DATA OF TEREPHTHALIC ACID STANDARDS	64
TABLE 6 RAW DATA OF PET CONVERSION RATE BASED ON WEIGHT PERCENTAGE (BM – BALL-MILLED PET SAMPLES; FR – FRESH PET SAMPLES; PH – PHOTOAGED PET SAMPLES; 1HR – 1 - HOUR RETENTION TIME; 2HR – 2 - HOUR RETENTION TIME).	66
TABLE 7 RAW DATA OF TPA YIELD BASED ON WEIGHT PERCENTAGE (BM – BALL-MILLED PET SAMPLES; FR – FRESH PET SAMPLES; PH – PHOTOAGED PET SAMPLES; 1HR – 1 - HOUR RETENTION TIME; 2HR – 2 - HOUR RETENTION TIME).	66
TABLE 8 RAW DATA OF TPA YIELD BASED ON WEIGHT PERCENTAGE (BM – BALL-MILLED PET SAMPLES; FR – FRESH PET SAMPLES; PH – PHOTOAGED PET SAMPLES; 1HR – 1 - HOUR RETENTION TIME; 2HR – 2 - HOUR RETENTION TIME).	67

TABLE 9 RAW DATA OF PET CONVERSION RATE, YIELD OF TPA AND YIELD OF EG.....	67
TABLE 10 RAW DATA OF XRD PEAK FITTING.....	68

List of Figures

FIGURE 1 FROM 2010 TO 2025, THE ESTIMATED CUMULATIVE AMOUNTS OF OCEAN WASTE PLASTICS IN MILLIONS OF TONS FROM JAMBECK ET AL. (2015) [2].....	1
FIGURE 2 MSW PRODUCTION RATES (KG/PERSON/DAY) AROUND THE WORLD FROM KAZA ET AL. (2018) [5].	2
FIGURE 3 POTENTIAL TRANSPORTATION PATHWAYS AND BIOLOGICAL INTERACTIONS OF OCEANIC PLASTIC WASTE FROM LI, TSE, & FOK (2016) [14].	3
FIGURE 4 CHEMICAL STRUCTURES AND CHEMICAL BONDS BETWEEN MONOMERS OF VARIOUS WASTE PLASTICS IN THE WORLD ADAPTED FROM GU & OZBAKKALOGLU (2016) [19].....	4
FIGURE 5 REACTION STOICHIOMETRY OF PET HYDROLYSIS ADAPTED FROM PASZUN & SPYCHAJ (1997) [26].....	5
FIGURE 6 REACTION PATHWAYS OF PET RECYCLING IN SUPERCRITICAL OR SUBCRITICAL WATER ADAPTED FROM SATO ET AL. (2006) [21].....	7
FIGURE 7 OUTCOMES OF PET RECYCLING IN SUPERCRITICAL OR SUBCRITICAL WATER FROM SATO ET AL. (2006) [21].....	8
FIGURE 8 A PET NEUTRAL HYDROLYSIS MODEL FROM ZOPE & MISHRA (2008) [39].	9
FIGURE 9 THE STRUCTURE OF SEMI-CRYSTALLINE POLYMER FROM DEMIREL ET AL. (2011) [42].....	11
FIGURE 10 THE XRD SPECTRA OF SEMI-CRYSTALLINE PET AT VARIOUS DURATIONS OF BALL-MILLING TIME FROM BAI ET AL. (2000) [27].....	12

FIGURE 11 GENERALIZATION EXPERIMENT PROCEDURES OF PET HYDROLYSIS.	15
FIGURE 12 A STAINLESS-STEEL CYLINDER AND STAINLESS-STEEL BALLS FOR BALL MILLING.	16
FIGURE 13 SCHEMATICS OF PET HYDROLYSIS CONSISTING OF A BATCH REACTOR, A WATER BATH PART, A SAND BATH PART, AND A PULLEY SYSTEM.	20
FIGURE 14 KEY PARTS OF TUBE HYDROLYSIS REACTORS: PRESSURE GAUGE, REACTOR BODY AND THE STAINLESS-STEEL DISC-SHAPED HOLDER.	21
FIGURE 15 APPEARANCE OF SOLUTIONS WHILE RECOVERING TPA: SOLUTION AFTER ADDING SODIUM HYDROXIDE (LEFT), AND SOLUTION AFTER ADDING HYDROCHLORIC ACID (RIGHT).....	23
FIGURE 16 REACTION STOICHIOMETRY FOR RECOVERING TEREPHTHALIC ACID IN SOLID PHASE ADAPTED FROM KARAYANNIDIS ET AL. (2002) [25].	24
FIGURE 17 XRD DIFFRACTOGRAMS OF PROGRESSIVELY BALL-MILLED PET SAMPLES: (A) BLUE: BALL-MILLED PET AFTER 70 MIN, (B) GREEN: BALL- MILLED PET AFTER 35 MIN, (C) RED: BALL-MILLED PET AFTER 12 MIN, (D) GREEN: FRESH PET.	29
FIGURE 18 DEVOLUTION OF XRD SPECTRA FOR THE ESTIMATION OF PET CRYSTALLINITY.....	30
FIGURE 19 DEGREE OF CRYSTALLINITY FOR UNPRETREATED PET SAMPLES, 35- MIN BALL-MILLED PET SAMPLES AND 70-MIN BALL-MILLED PET SAMPLES..	31
FIGURE 20 RAMAN SPECTRA OF FRESH PET AND PHOTOAGED PET.....	32
FIGURE 21 FT-IR SPECTRA OF FRESH PET AND PHOTOAGED PET.....	33

FIGURE 22 SCANNING ELECTRON MICROSCOPY (SEM) IMAGES OF SAMPLE: A (UNPRETREATED PET), IMAGE B (BALL-MILLED PET (12MIN)), IMAGE C (BALL- MILLED PET (70MIN)), AND IMAGE D (PHOTOAGED PET (AFTER 12MIN BALL- MILLING)).	34
FIGURE 23 THERMOGRAVIMETRIC ANALYSIS (TGA) CURVES OF RECOVERED TEREPHTHALIC ACID (TPA) FROM HYDROLYZED SOLID PRODUCTS AND STANDARD TPA.	35
FIGURE 24 DTG (DERIVATIVE THERMOGRAVIMETRIC) CURVES OF RECOVERED TPA FROM HYDROLYZED SOLID PRODUCTS AND STANDARD TPA.	36
FIGURE 25 FT-IR SPECTRA OF RECOVERED TPA FROM HYDROLYZED SOLID PRODUCTS AND STANDARD TPA.	37
FIGURE 26. UV-VISIBLE CURVES OF RECOVERED TPA FROM HYDROLYZED SOLID PRODUCTS AND STANDARD TPA.	38
FIGURE 27 HPLC CURVES OF RECOVERED TPA FROM HYDROLYZED SOLID PRODUCTS AND STANDARD TPA.	39
FIGURE 28 DEPOLYMERIZATION OF PET AT DIFFERENT REACTION CONDITIONS: PET CONVERSIONS AT 20 MIN AND DIFFERENT REACTION TEMPERATURES; PET CONVERSIONS AT 200 °C AND DIFFERENT RETENTION TIMES.	40
FIGURE 29 THE REARRANGED LINEAR EQUATION OF PET HYDROLYSIS AT SUBCRITICAL WATER OBTAINED FROM THE ARRHENIUS EQUATION.	42
FIGURE 30 PET CONVERSION RATE, TPA YIELD AND EG YIELD OF UNPRETREATED PET SAMPLES AND BALL-MILLED PET SAMPLES (70MIN) AFTER A REACTION TIME OF 1 HOUR.	45

FIGURE 31 PET CONVERSION RATE, TPA YIELD AND EG YIELD OF UNPRETREATED PET SAMPLES AND BALL-MILLED PET SAMPLES (70MIN) AFTER A REACTION TIME OF 2 HOUR.	46
FIGURE 32 PET CONVERSION RATE, TPA YIELD AND EG YIELD OF UNPRETREATED PET SAMPLES AND PHOTOAGED ET SAMPLES (70MIN) AFTER A REACTION TIME OF 1 HOUR.	48
FIGURE 33 CALIBRATION OF ETHYLENE GLYCOL.	63
FIGURE 34 CALIBRATIONS OF TPA: (A) CALIBRATION OF TPA (ABS>1.0), (B) CALIBRATION OF TPA (0.6 < ABS < 1.0), (C) CALIBRATION OF TPA (0.3 < ABS < 0.6).	65
FIGURE 35 FT-IR SPECTRUM OF RECOVERED TPA FROM HYDROLYZED SOLID PRODUCTS AND STANDARD TPA (FRESH PET, 1 HOUR).	69
FIGURE 36 FT-IR SPECTRUM OF RECOVERED TPA FROM HYDROLYZED SOLID PRODUCTS AND STANDARD TPA (FRESH PET, 2 HOURS).	69
FIGURE 37 FT-IR SPECTRUM OF RECOVERED TPA FROM HYDROLYZED SOLID PRODUCTS AND STANDARD TPA (BALL-MILLED PET, 1 HOUR).	70
FIGURE 38 FT-IR SPECTRA OF RECOVERED TPA FROM HYDROLYZED SOLID PRODUCTS AND STANDARD TPA (BALL-MILLED PET, 2 HOURS).	70

Part 1 Introduction

Plastic waste in the ocean has become a pressing issue for the sea, physical health, and society. With the improving plastic consumption along with population growth, an increasing number of wastes marine plastics were generated and buried in the ocean. These wastes plastics have negatively affected human-beings, wildlife, and wildlife habitats [1]. Enhancements of waste management infrastructures are necessary now. It is estimated that from 2010 to 2025, the cumulative amount of marine plastic waste will increase by orders of magnitude [2].

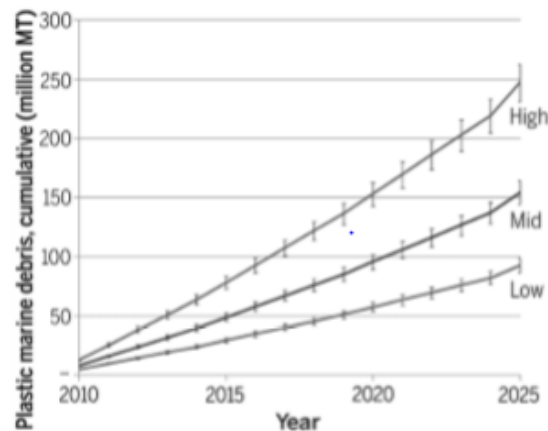


Figure 1 From 2010 to 2025, the estimated cumulative amounts of ocean waste plastics in millions of tons from Jambeck et al. (2015) [2].

Ocean plastic waste, one of the main compositions in municipal solid wastes (MSW), has led to raising the attention of waste management [3]. MSW is the most common and complicated solid waste stream resulting from human activities, including agricultural and industrial productions [4]. The management of municipal solid waste influences every person around the world. By 2050, increase waste generation is expected to increase by 70 percent in the world, from 2.01 billion tons of waste in 2016 to 3.40 billion tons of waste [5]. Waste management is a complicated issue,

including plan making, contracting management and monitoring operations. [5, 6] **Figure 2** has shown the MSW production rate for 23 low- and middle-income countries compared to US and EU [5].

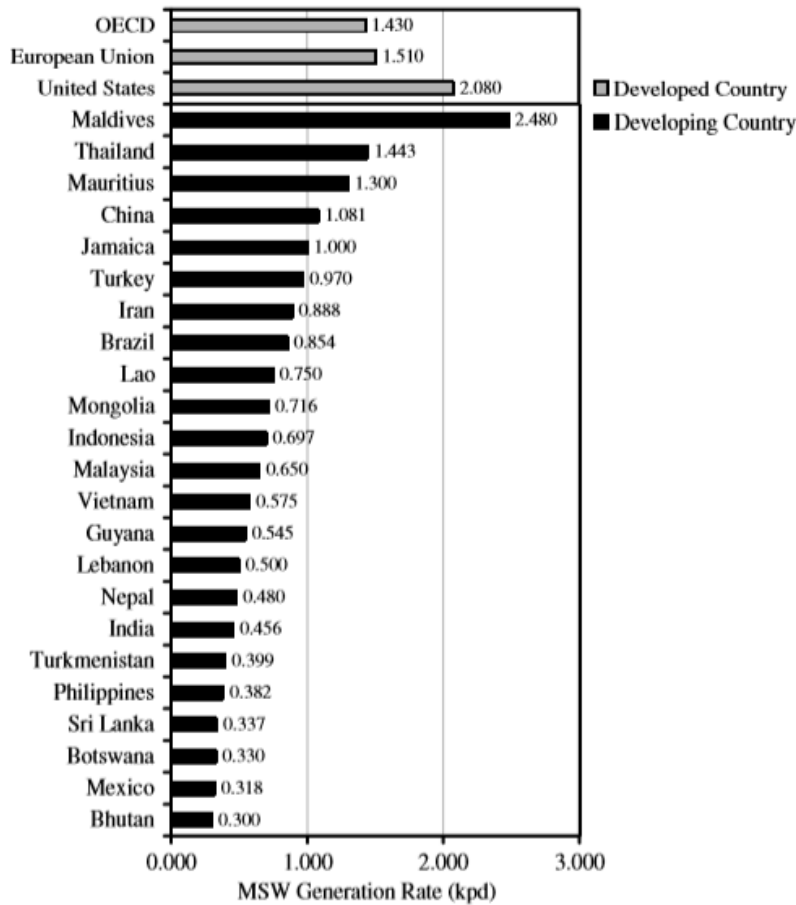


Figure 2 MSW production rates (kg/person/day) around the world from Kaza et al. (2018) [5].

Recovering solid wastes is one of the critical elements in dealing with MSW [7]. Currently, an increasing number of countries have been developing new technologies for the reprocessing of solid wastes. The economic considerations of solid wastes vary across nations. Technologies for collecting, reprocessing, and disposing of MSW is essential to address environmental and economic problems [8]. In the USA, nearly 30% of MSW was recovered [9].

Plastics, as a critical component of solid waste, are suitable to be recycled [10]. Synthetic polymers have become an essential part of the natural environment, and also have disastrous effects on the ocean environment. Plastic contamination in the ocean environment has gradually attracted attention from industries and general. For decades, oceanic garbage has been regarded as a global environmental concern [11-13].

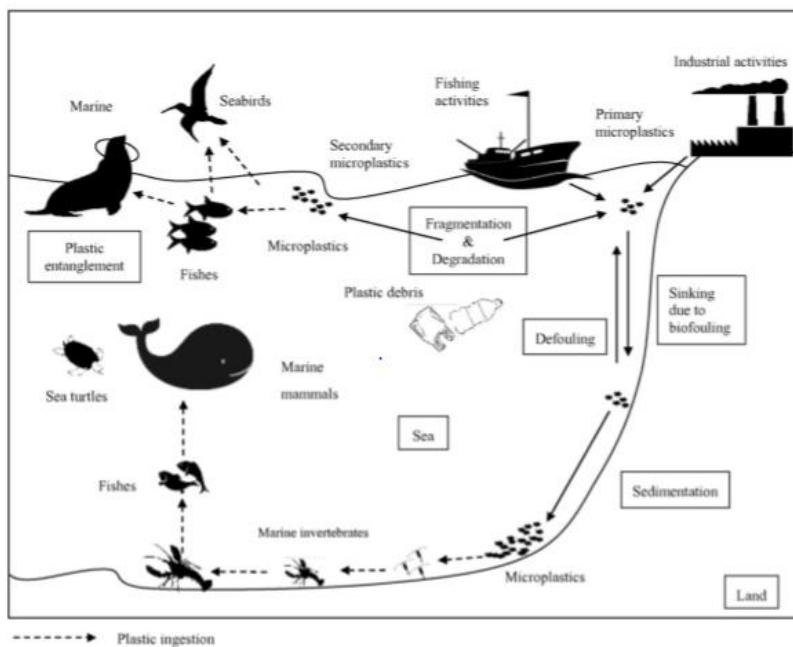


Figure 3 Potential transportation pathways and biological interactions of oceanic plastic waste from LI, Tse, & Fok (2016) [14].

However, synthetic polymers, commonly known as plastics, are not easy to be degraded by environmental degradation. Finding an effective and economical approach to degrade oceanic plastics is in demand now. Improvements in managing oceanic plastic waste are critical to reducing plastic pollution [15]. Alternatively, polymeric materials obtained from the ocean can be converted into commercialized chemicals and fuels [16].

Plastic hydrolysis technology is an environmentally friendly method for recovering commercialized organics from waste plastics. Owing to its high energy efficiency and cost-effectiveness, it has become a promising approach for degrading plastics [17, 18]. Most commonly-used or commercialized synthetic polymers are polystyrene (PS), polyvinyl chloride (PVC), polypropylene (PP), high-density polyethylene (HDPE), low-density polyethylene (LDPE) and polyethylene terephthalate (PET) [19]. The molecular structures of these plastics have been shown in **Figure 4**.

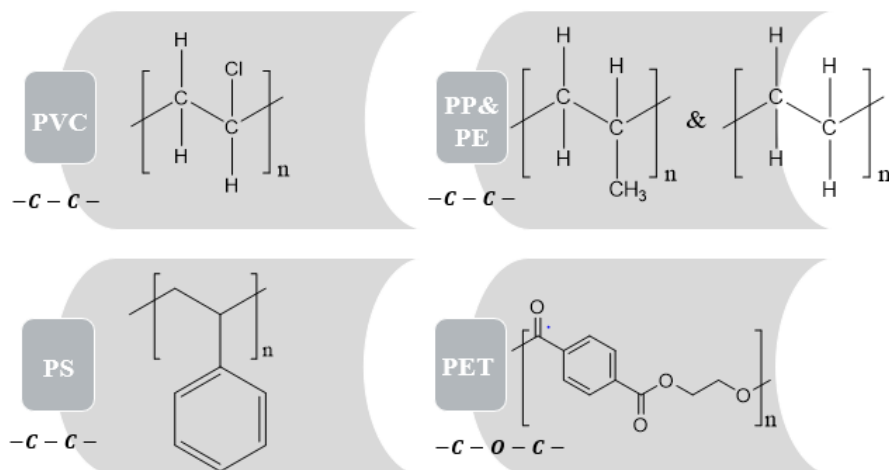


Figure 4 Chemical structures and chemical bonds between monomers of various waste plastics in the world adapted from Gu & Ozbakkaloglu (2016) [19].

Chemical degradation of polymers synthesized from hydrocarbons requires higher temperatures at hot compressed water [20]. Unlike most plastics, polyethylene terephthalate monomers are connected by an ester linkage, which allows PET to be degraded at lower temperatures by hydrolysis [21]. In general, hydrolysis of PET has become a greener route for chemical recycling [22].

PET hydrolysis is also an economic waste chemical reprocessing method because of its cost-effectiveness [23]. PET can be hydrolyzed into its monomers, which makes it possible for chemical recycling. Due to the economic and ecological considerations, growing interests in finding an effective approach to degrade PET makes PET recycling important. In subcritical water or supercritical water, PET can be hydrolyzed to TPA and EG [21, 24-26].

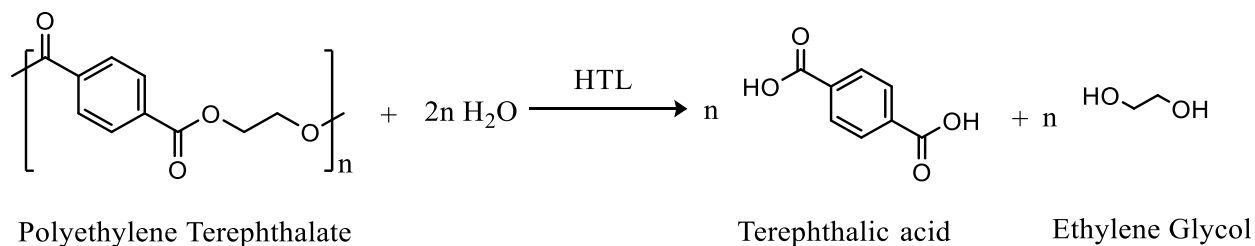


Figure 5 Reaction stoichiometry of PET hydrolysis adapted from Paszun & Szychaj (1997) [26].

A wide range of research topics related to the hydrolysis of PET have been studied. Because oceanic plastics experience environmental degradation such as oxidation, mechanical stress, and radiation damage, the mechanical features and chemical properties may be different from fresh plastics [27-29]. Cellulose, the natural polymer found abundantly in plants, can be hydrolyzed to generate fuels and chemicals. Ball-milling treatments were found effective in decreasing cellulose crystallinity and increasing cellulose hydrolysis reactivity [30]. Ball milling may also have similar effects on polyesters, including PET. To understand the chemical and physical properties of waste plastics, performing HTL experiments of ball-milled PET and photoaged PET is a good start for understanding the reactivity and structures of ocean plastics.

Part 2 Background

2.1 Chemical recycling of Poly (ethylene terephthalate)

2.1.1 Methods for recovering TPA and EG from PET

Polyethylene terephthalate is a type of polyester synthesized by ethylene glycol (EG) and terephthalic acid (TPA) [21, 22, 26, 31]. Polyethylene terephthalate also plays a critical role in maintaining food quality, safety, and alleviating food waste [32]. Chemical recycling of wastes plastics such as PET can be performed in different methods, including pyrolysis, hydrolysis, alcoholysis, acidolysis, aminolysis, etc. The dominant PET degradation mechanism is the ester linkage solvolysis. Water, alcohol, acid, or alkali are suitable solvolytic agents for PET degradation [26].

Hot compressed water or glycol are suitable solvents for breaking ester linkages [24]. Compared to glycol, depolymerization of PET by using hot compressed water such as hydrolysis is an environmentally friendly treatment for recycling PET monomers. It also avoids using organic solvents like alcohol or glycol, eliminating organic solvents from technological cycles [26].

Chemical recycling of PET has been established and studied for the cost-effective application of recycled products, terephthalic acid, as well as ethylene glycol [22, 26]. Terephthalic acid can be used to manufacture polyesters [33]. As an essential chemical intermediate and organic compound, ethylene glycol, the main product in liquid fraction, has been widely applied in engineering processes such as energy, plastics, chemicals, and automobiles [34]. **Figure 6** adapted from Sato et al. (2006) has shown that recovering and recycling commercialized chemicals from PET hydrolysis is achievable.

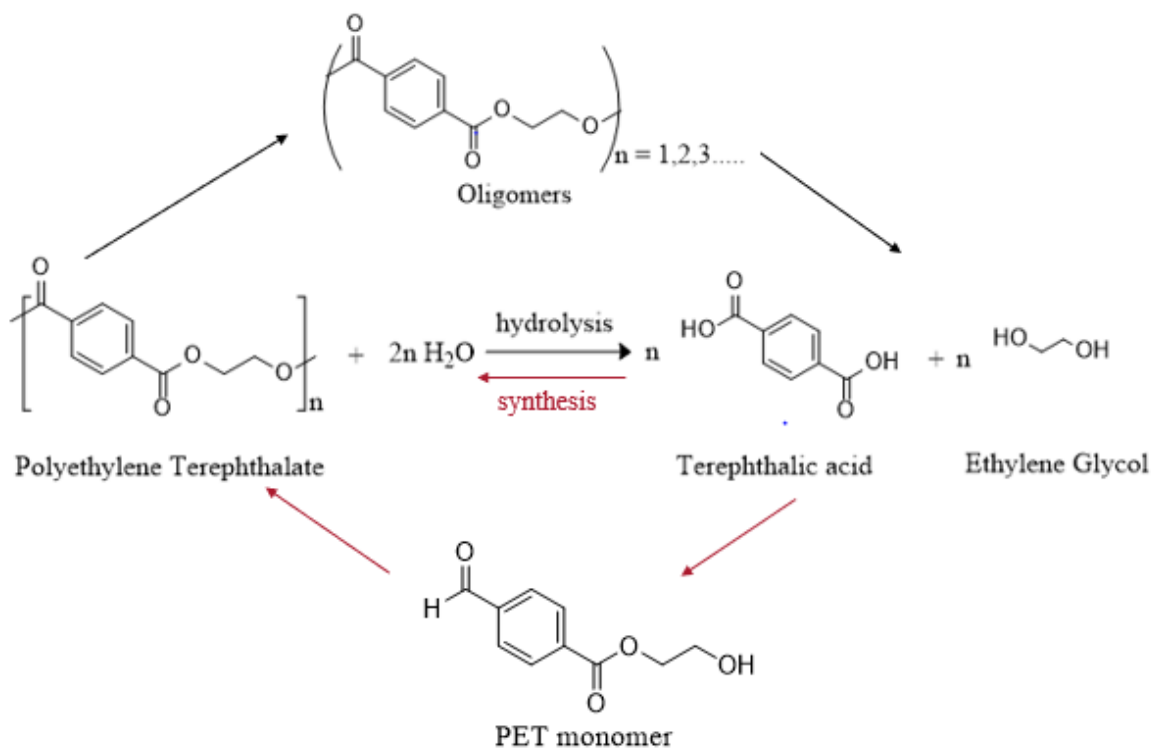


Figure 6 Reaction pathways of PET recycling in supercritical or subcritical water adapted from Sato et al. (2006) [21].

2.1.2 Chemical recycling of PET by hydrolysis

PET hydrolysis can be mainly carried out in four ways: acid hydrolysis, alkaline hydrolysis, catalytic hydrolysis, and neutral hydrolysis [25, 31, 35, 36]. Sulfuric acid was used to hydrolyze PET [37]. PET alkaline hydrolysis was carried out using the sodium hydroxide solution [36]. The main drawback of PET hydrolysis in acidic or basic environment is the high corrosivity of the reaction systems. It also produced tons of wastes, including contaminated water and inorganic wastes [26].

Catalytic hydrolysis of polyethylene terephthalate can take place at lower temperatures compared to neutral hydrolysis. The yields of TPA or EG can be higher at the same reaction temperatures

and retention time. With the existence of zinc acetate, depolymerization of PET was accelerated. The maximum yield of TPA was up to 90.5% at 240 °C [38].

2.2 Depolymerization of PET by using water at higher temperatures

2.2.1 Depolymerization behavior of neutral hydrolytic depolymerization of PET

The neutral hydrolytic depolymerization was usually performed at high temperatures. With the existence of water or steam, neutral hydrolysis takes place at higher temperatures ranging from 200 to 300 °C [26]. Growing interests in studying PET hydrolysis revealed that PET was hydrolyzed faster in the molten state rather than the actual state [22].

Recovering monomers from PET hydrolysis should be an ideal approach. For the chemical recycling of PET, the corresponding amounts or yields of terephthalic acid and ethylene glycol should be generated [21, 22]. Nevertheless, the ethylene glycol yield was always lower than the terephthalic acid yield for PET hydrolysis [35].

PET●; oligomer○; TPA▼; EG■.

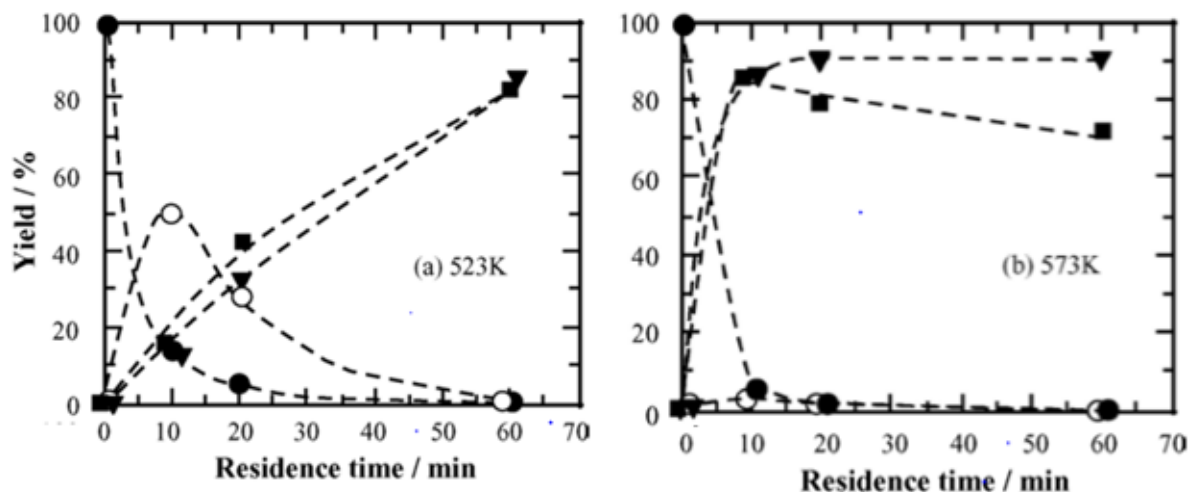


Figure 7 Outcomes of PET recycling in supercritical or subcritical water from Sato et al. (2006) [21].

The effect of proton is studied to understand why the chemical yield of ethylene glycol is lower [21]. Sato et al. (2006) also studied the depolymerization behavior of polyethylene terephthalate in hot compressed water. The outcomes of oligomers decreased with longer retention time. Chemical yields as a function of time and temperature have been shown in **Figure 7** [21].

2.2.2 Reaction kinetics of PET hydrolysis

Zope et al. (2008) have studied the reaction kinetics of PET hydrolysis at high temperature. A model of neutral hydrolytic depolymerization of used PET at high temperatures is investigated. The yield of terephthalic acid and the conversion of PET were measured during the hydrolysis of PET. The conversion rate of PET was increased at 200 °C with increased reaction time. With the increasing particle size, the amount of TPA obtained decreased, and the simultaneous fragmentation and depolymerization model explained this in **Figure 8** [39].

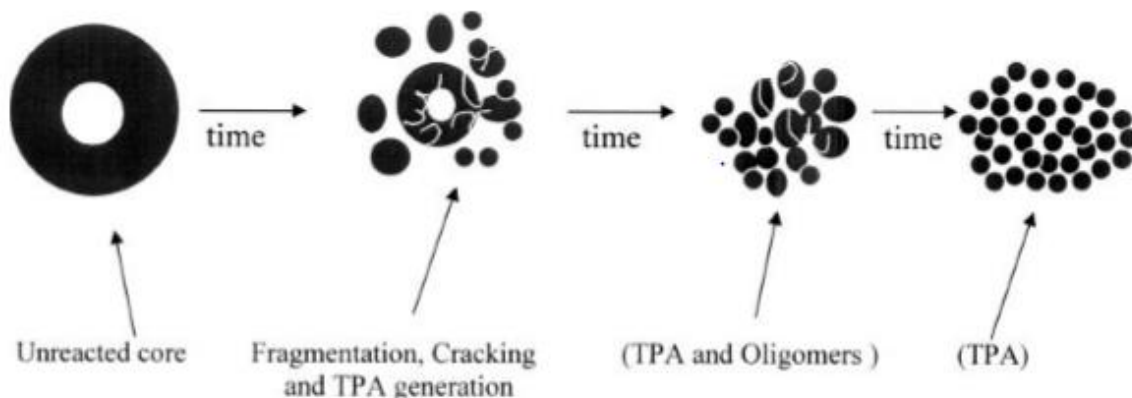


Figure 8 A PET neutral hydrolysis model from Zope & Mishra (2008) [39].

2.3 Structural features of PET and its measurement methods

2.3.1 Crystallinity of PET

The structure of polymeric materials is relatively complicated compared to other commonly used materials such as ceramics, glasses, and metals [40]. Most polymeric materials share two structural features between ceramics and glasses, and polymeric materials are challenging to be crystallized [41]. Common plastics have a large degree of non-crystallinity compared to metals and ceramics since producing the repeating patterns of long molecular chains is not easy [28].

Demirel, Yaraş, and Elçiçek (2011) revealed polyethylene terephthalate has partly crystalline structures since it is regular in chemical and geometry patterns. The repeating units lead to complicated molecular structures. The crystallization behavior of polyethylene terephthalate is same as most polymers, which exist as complicated molecular structures consisting of amorphous and crystalline fractions [42].

Most commercialized polyethylene terephthalate has the crystalline structure since the polymer chains are paralleled and closely packed, and the amorphous structure means that polyethylene terephthalate contains more disordered polymer chains [43]. Therefore, the degree of PET crystallinity is not 100% and lower. **Figure 9** showed this unique structure of polymers or polyethylene terephthalate called “semi-crystalline.”

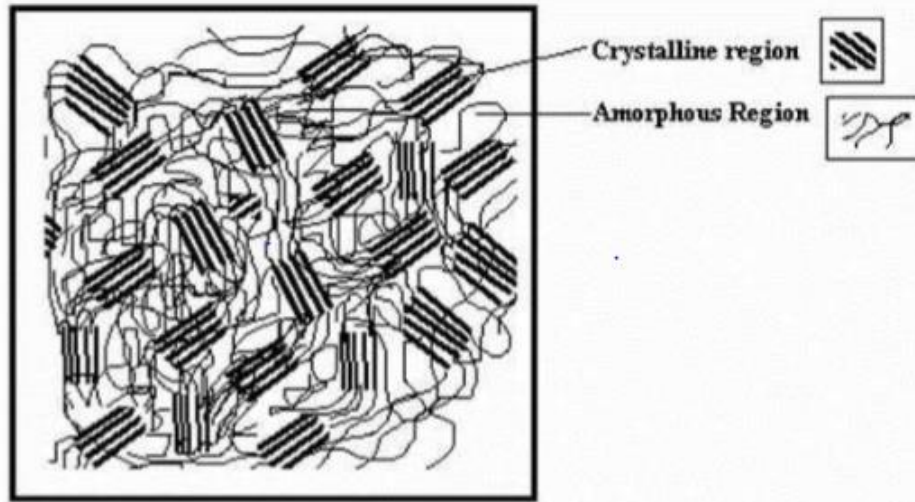


Figure 9 The structure of semi-crystalline polymer from Demirel et al. (2011) [42].

2.3.2 XRD measurement of PET crystallinity

The structural features of polymeric materials are relatively complex. Most polymeric materials have a complex structure composed of the amorphous and crystalline regions [44]. Generally, the properties of semi-crystalline polymers are determined by the degree of crystallinity, the order and size of the molecular chains and the fraction of the oriented molecules in polymers is defined as the degree of crystallinity [45].

PET is a kind of semi-crystalline polymers because of its regularity in geometric patterns. Commonly, the crystallinity and morphology can influence the properties of polymers dramatically. It is not only in the semi-crystalline state, but also in the amorphous state [45]. The XRD diffraction diagram of semi-crystalline PET is made up of the amorphous structural regions and the crystalline structural regions. The degree of PET crystallinity is commonly quantified by XRD because of its consistency and reliability in measuring crystallinity. Usually, the spectra of polymers were resolved into two major parts, regions of crystalline bands and a region of an

amorphous halo. Gaussian function was an effective model, which was used to estimate the area of the amorphous region and the total area [46].

2.3.3 Crystallization Behavior of PET and Mechanical Milling

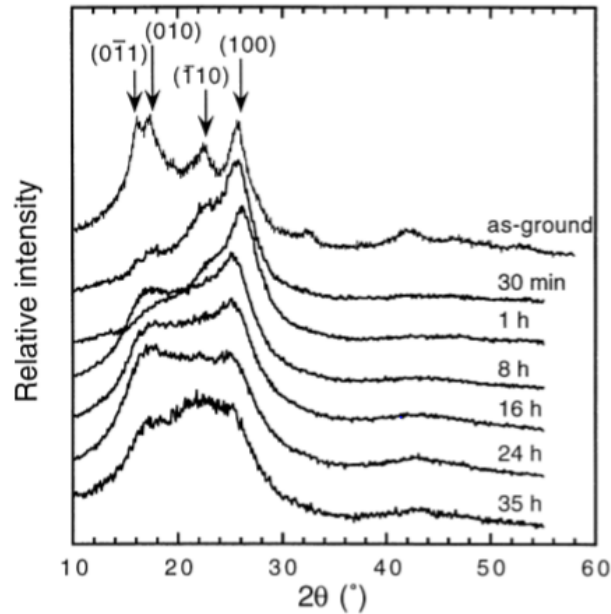


Figure 10 The XRD spectra of semi-crystalline PET at various durations of ball-milling time from Bai et al. (2000) [27].

The crystallization behavior of polyethylene terephthalate is related to mechanical milling. Bai et al. (2000) discovered that structural changes in polymers could be induced by mechanical stress. High-energy ball milling, a kind of mechanical milling method, was an appropriate approach for changing the geometrical patterns or the mechanical properties of PET. Structural changes induced by mechanical milling were including: 1) the reduction in average particle size; 2) the decrease in molecular weight; 3) a reduction of apparent crystallinity with increasing milling time. In **Figure 10**, the XRD spectra of fresh PET and cool-milled PET for different durations indicated the effects of mechanical stress on PET crystallinity [27].

2.3.4 Photodegradation induced by ultraviolet light

The natural environment caused various chemical changes in polymeric materials, such as polyesters [47]. Photodegradation took place under solar light. Under the action of sunlight, PET photodegradation resulted in main degradation event including chain scission, leading to a decrease in molecular weight, evolution of volatile products, such as the evolution of CO and CO₂ as well as generation of carboxyl end-groups [48]. These degradation events took place under the action of sunlight. The strength of chemical bonds, including C–C, O–O, H–O, and C–N in polymers, is usually lower than the energy of ultraviolet light [49]. Chemical bonds in polymeric material are more likely to break with Ultraviolet light [50].

2.4 Characterizations and measurements of PET hydrolyzed products

2.4.1 TPA recovery

The main products of PET hydrolysis are ethylene glycol in the liquid fraction and terephthalic acid in the solid fraction. Terephthalic acid, which has a high melting point at 427 °C, is tough to be dissolved in non-basic solvents because of its low solubility [51]. Because of this, the recovery of terephthalic acid from the hydrolyzed products can be achievable by using basic solutions. During PET hydrolysis, oligomers of EG and TPA are produced as byproducts. Monoesters of EG and TPA are soluble in water at 95 to 100 °C. However, TPA cannot be dissolved in water at this temperature range, which makes it easier to obtain highly-purified TPA from postreaction products [31]. Terephthalic acid was recovered by dissolving it into the basic solution such as sodium hydroxide. The clear basic liquid was then neutralized by adding hydrochloric acid. TPA was obtained from the precipitated product [21].

2.4.2 Characterization and measurements of TPA

Ravichandran et al. (2016) developed a characterization method for quantitative and qualitative analysis of TPA monomer from recycled PET wastes. The final product in the solid phase, terephthalic acid, was characterized and measured by using Fourier transform-infrared spectroscopy (FT-IR), Thermogravimetric analysis (TGA) and UV-Visible spectrophotometry. The quantity and purity of PET hydrolyzed samples were analyzed by FTIR and TGA. Functional group analysis of TPA and hydrolyzed solid products were carried out by using FT-IR. Both quantitative and qualitative analysis was carried out by using UV-Visible spectrophotometry [52].

Part 3 Experiments

Experimental procedures were divided into three main sections. First, the pretreatment experiments of PET were performed to change the structural properties of PET. Second, tube hydrolysis reaction was performed for PET recycling, and end products were recovered after reactions. In the end, quantitative and qualitative analyses were carried out to obtain the chemical yields of end products and the conversion rate of PET. **Figure 11** has shown the entire experimental procedures of PET recycling by hydrolysis.

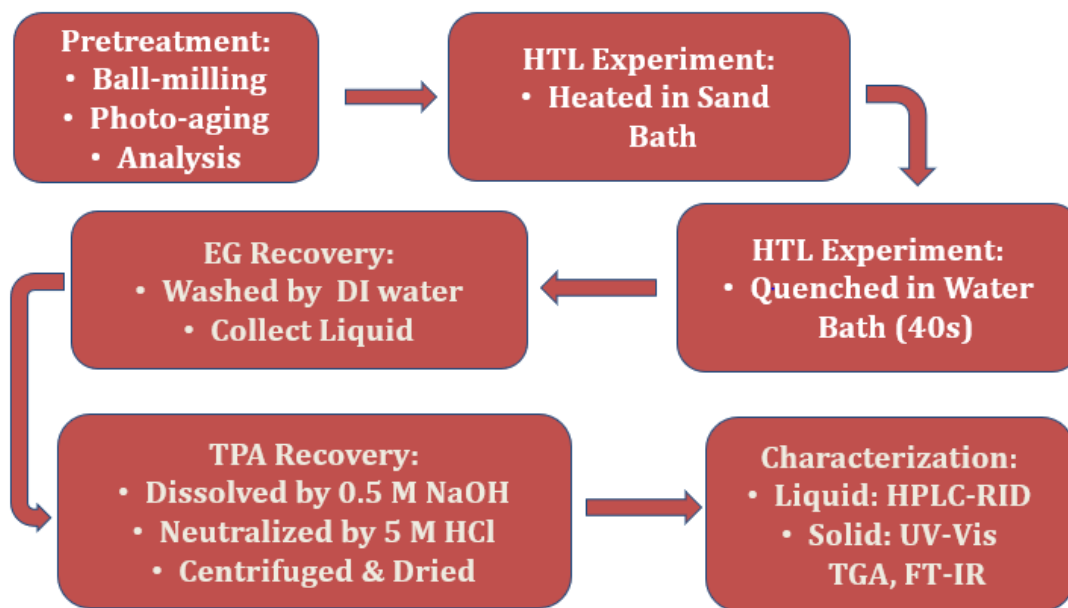


Figure 11 Generalization experiment procedures of PET hydrolysis.

3.1 Materials

Polyethylene terephthalate was supplied by Goodfellow Cambridge Limited (Huntington, England, PE29 6WR). Terephthalic acid was purchased from Sigma-Aldrich Corporation (Natick, MA, 98%

purity). Ethylene glycol was also purchased from Sigma-Aldrich Corporation (Natick, MA, 99.8% purity). Sodium hydroxide was supplied from Sigma-Aldrich Corporation (Natick, MA, $\geq 97.0\%$ purity, pellets), and hydrochloric acid was purchased from Sigma-Aldrich Corporation (Natick, MA, 36.5%-38.0% concentration).

3.2 Pretreatment of PET samples and characterizations

PET samples were pretreated by ball-milling and photoaging experiments to change the mechanical and chemical properties. Several instrumental analysis methods were applied to analyze the crystallinity, chemical bonds, and morphology of polyethylene terephthalate.

3.2.1 Mechanical milling of PET

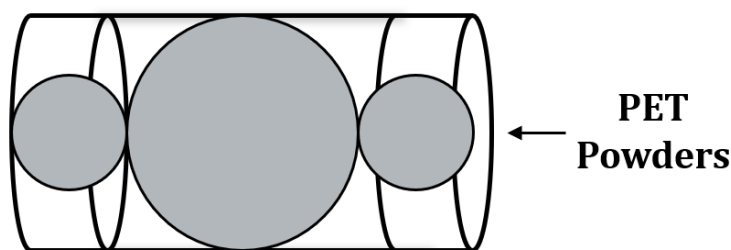


Figure 12 A stainless-steel cylinder and stainless-steel balls for ball milling.

Mechanical de-crystallization of semi-crystalline PET powders was carried out by a temperature-controlled ball-milling treatment at different lengths of time. PET samples of different degrees of crystallinity were produced by ball-milling. A stainless-steel cylinder (18 mm diameter \times 55.5 mm length, 10 mL) was used to place around 2.5 grams of PET powders. The cylinder contained inside two stainless-steel balls (9.5 mm diameter) and one relatively larger stainless-steel balls (15.85 mm diameter). Two cylinders were tightly clumped in the holder of a vibratory shaker (Retsch

MM2000) for ball-milling treatment. **Figure 12** has shown the structure of the cylinder for ball-milling.

PET powders were ball-milled at a duration time of 12, 35, and 70 minutes separately. While performing the ball-milling treatment, the temperature was controlled to prevent PET powders from melting. To keep PET powders at the same temperature as the ambient temperature, all samples were ball-milled for 1 to 3 minutes and then were stopped for more than 10 minutes to cool down. This process was repeated until accumulating the total milling time of the set durations. This ball-milling treatment method was applied to avoid the effect of frictional heat on polymer structure.

3.2.2 X-ray diffraction (XRD)

To estimate the degree of crystallinity for PET, X-Ray diffraction (XRD) patterns were carried out with Cu K α radiation at 25 mA and 37.5 kV on an X-ray Powder Diffractometer (Geigerflex, Rigaku Co., Tokyo, Japan) with the Bragg-Bretano theta-theta configuration. Each spectrum of PET under various pretreatments was resolved into an amorphous halo and the whole region under the diffraction curve line.

A step size of 0.02° was used with 1 second accumulation time for XRD measurements over a range of 6-60°. After normalizing the areas and subtracting the baseline, diffractograms of various PET samples were compared. The Magic Plot program was used for all the peak-fitting steps.

3.2.3 Radiation damage

PET samples were incubated in a solar simulator (Atlas Suntest CPS+, Atlas Material Testing Technology LLC) set at 765 W/m². The irradiance of this incubation experiment was equal to a 96-hour incubation treatment of natural sunlight in the Gulf of Mexico [53].

3.2.4 Chemical-bond analysis: Raman microscopy and FT-IR

Chemical bonds in polyethylene terephthalate were characterized by using Raman microscopy and Fourier transform-infrared spectroscopy (FT-IR).

Analysis of Raman spectra of PET samples was performed with a Horiba Xplora Raman Microscope using 532 nm excitation laser with an operation condition: 100× Olympus magnification lens, 1800 gratings, and 10% power. Approximately 50-100 mg samples were placed onto the glass slides for Raman microscopy. Three spots were chosen for unpretreated PET samples and photoaged PET samples separately. All the three Raman spectra were averaged and normalized for each kind of PET samples. After normalizing and averaging the Raman spectra, a spectrum of fresh PET and a spectrum of photoaged PET were compared.

FT-IR spectral analysis was carried out for the analysis of chemical functional groups in polyethylene terephthalate. Both unpretreated PET and photoaged PET samples were characterized by using a Spectrum Two FT-IR spectrophotometer (PerkinElmer, MA, USA) that was coupled with a crystal reflection cell. The transmittance mode of FT-IR analysis was used over a range of 4000 to 400 cm^{-1} . Around 10-30 mg PET samples were placed onto the crystal surface. Later, PET samples were pressed into the crystal head.

3.2.5 Scanning electron microscopy (SEM)

The morphology of unpretreated, ball-milled, and photoaged PET samples were characterized by using scanning electron microscope (SEM) (JSM 7000F SEM, JEOL Ltd., Tokyo, Japan). SEM images of various PET samples were compared.

3.3 Tube hydrolysis reactor experiment

Tubular batch reactors and a reaction system were constructed for PET hydrolysis. Reactor constructions and safety considerations were specified in the first place of this chapter. Experimental procedures of PET hydrolysis and recovery of end products were also included.

3.3.1 Reactor constructions and safety considerations

The reaction system for this hydrothermal liquefaction experiment was mainly consisting of four parts: a batch reactor for the reaction, a water bath part for the quenching process, a sand bath for the heating step, and a pulley system for controlling the position of the batch reactor. The experiment setup for PET hydrolysis is shown in **Figure 13**.

The batch reactor body for PET hydrolysis was built from a 316 stainless steel Swagelok tube (1/2 × 0.065 in.). This reactor was placed in a heating/cooling system during the degradation, and high-temperature and high-pressure experiments were carried out in tube hydrolysis reactors. The reaction conditions for this experiment were at a temperature range of 200 ~ 270°C and a time range of 10 ~ 120 min.

This small-scale batch reactor was built to test the reactivity of PET with various pretreated methods. Without considering the complex reactions or operations and the massive weight of feedstocks, CSTRs were not required for PET hydrolysis. Owing to the small scales of tube hydrolysis reactors, problems related to heat transfer, toxic gaseous chemicals, and operations can be neglected. Parameters of building these tube hydrolysis reactors are listed in **Appendix A**.

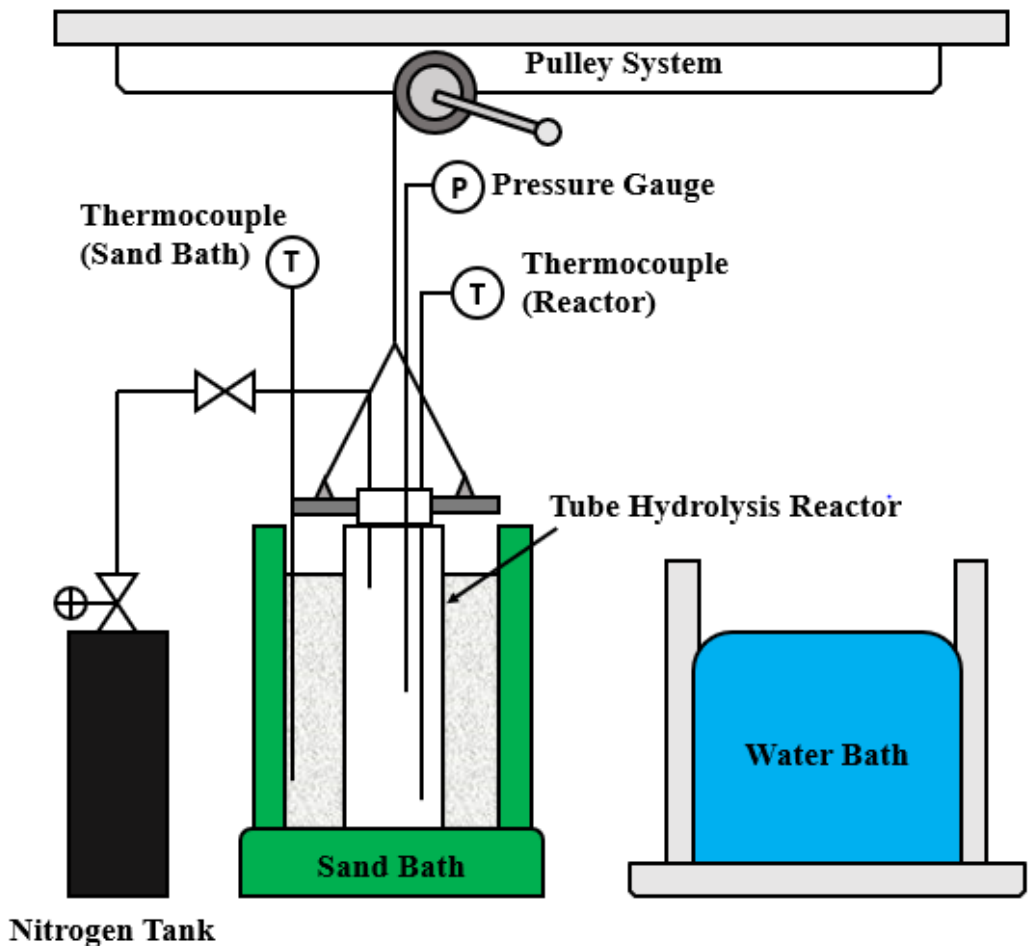


Figure 13 Schematics of PET hydrolysis consisting of a batch reactor, a water bath part, a sand bath part, and a pulley system.

Two important steps were specified as follows to avoid the leaking issues of the tube reactors. First, after uploading the feedstocks, the reactor body must be tightened clockwise till the nut fit the seal tightly. Second, after sealing the reactor, another step called monitoring the pressure was required to make sure the reactor was leak-free.

When the reactors were well-sealed, the tube hydrolysis reactors were placed onto the hook in the enclosure, preventing it from falling down while operating the pulley system. The second step, called monitoring the pressure, was performed after the sealing step. Tube reactors were

pressurized to 1000 psi by using nitrogen and then held for nearly 20 minutes. There should be no bubbles generated while using SNOOP to check every connecting parts of tube reactors. Also, the SNOOP is helpful for finding the leak. If the pressure does not decrease after the holding time, the reactors should be leak-free. **Figure 14** has shown the images of key parts of tube hydrolysis reactors.



Figure 14 Key parts of tube hydrolysis reactors: pressure gauge, reactor body and the stainless-steel disc-shaped holder.

Prior to the hydrothermal reaction, all the air inside the tube hydrolysis reactors should be cleared out by using nitrogen for more than three times. The initial reaction pressure was 500 psi by using nitrogen. The reactors were well-prepared to be dropped into the sand bath for reaction.

3.3.2 Hydrothermal experiment of PET in the tubular reactors

PET hydrolysis was carried out under the high-temperature and high-pressure conditions. Around 0.30-0.33 g PET samples and 4 grams of DI water were uploaded into the tubular reactor. The PET

samples for reactions including the original PET, ball-milled PET (70min), and photoaged PET. Hydrolysis of PET in subcritical water was then performed in a stainless-steel tubular reactor.

The reactor was placed on a stainless-steel disc-shaped holder. After uploading the feedstocks, the reactor was submerged into a sand bath. The temperature was controlled at 200 °C, and the retention time was 1 hour or 2 hours. Four minutes was required for the whole reactor to reach the reaction temperature, and the ramping up time was not included in the retention time. When the reaction was finished, the reactor was rapidly taken out from the sand bath by a pulley system. After this step, the reactor was immediately quenched in a water bath and then cooled down to 20 °C for 1 minute. The cooled reactor was taken out and opened for the following procedures.

3.3.3 Recovery procedures of end products

Recovered products from the degraded PET samples were divided into the aqueous phase products and the solid phase products. The water-soluble liquid and solid fractions were washed into a 50 ml centrifuge bottle by DI water after the reaction. 40-50 ml DI water was used to ensure all the water-soluble products and solid fractions can be collected into the same centrifuge bottle. The mass of an empty centrifuge bottle (mass A) and the total mass of a centrifuge bottle filled with products and DI water (mass B) were recorded by weighing them on the same analytical balance.

All separation processes of liquid and solid fractions were carried out by using a centrifuge (SORVALL LEGEND RT+). All samples were separated in a centrifuge for 20 minutes at 22°C with a centrifugal speed of 3000 rpm. Approximately 10-12 grams of liquid sample was collected into a vial for HPLC analysis. The centrifuge bottles were dried in an oven at 60°C for two days. The mass of the centrifuge bottle and solid fractions (mass C) were recorded. The mass of liquid A (mass D) was then obtained by subtracting the difference from mass B to mass C, and the mass

of solid was obtained by subtracting the difference from mass B to mass A. Ethylene glycol was recovered in the aqueous phase products (liquid A).

Recovering terephthalic acid was more complicated compared to the recovery procedures of ethylene glycol. Recovery procedures of TPA took use of an acid-base reaction, a neutralization reaction [25]. TPA can be dissolved in basic solutions such as sodium hydroxide, and a clear solution was formed after the dissolution. The appearance of the white slurry was formed when acid solutions were dropped into the clear alkaline solution. Hydrochloric acid or sulfuric acid solutions are commonly applied to recovering TPA. **Figure 15** showed the appearance of solutions after adding a basic solution and acidic solution while recovering PET.



Figure 15 Appearance of solutions while recovering TPA: solution after adding sodium hydroxide (left), and solution after adding hydrochloric acid (right).

The main product in the dried solids, terephthalic acid, was dissolved in around 40 ml 0.5 M sodium hydroxide solution and then separated into NaOH-soluble phase and solid phase.

Separation processes were also performed by using the centrifuge. After separating the NaOH-soluble products from the solid fraction (unreacted PET), around 10 ml of basic solution were taken out for UV analysis to obtain the yield of TPA. Extra clear solution was then neutralized with 5 M hydrochloric acid. The chemical reaction of the second-step separation process was shown in **Figure 16**. Terephthalic acid was obtained. The recovered terephthalic acid was dried for more than 48 hours for the characterization of TGA and FT-IR. The unreacted PET was also dried for more than 48 hours for obtaining the conversion rate of PET.

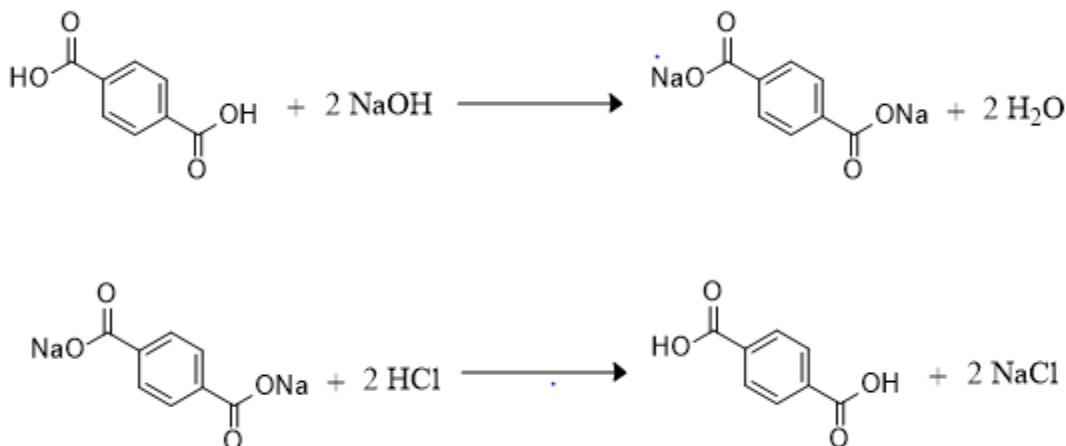


Figure 16 Reaction stoichiometry for recovering terephthalic acid in solid phase adapted from Karayannidis et al. (2002) [25].

3.4 Analysis of end products

Analysis of recovered liquid products was carried out by using High-Performance Liquid Chromatography (HPLC). Characterization of recovered solid products was performed by applying Thermogravimetric Analysis (TGA), Fourier transform-infrared spectroscopy (FT-IR), and UV-Visible spectrophotometer.

3.4.1 Analysis of UV-Visible spectrophotometer

UV-Visible spectrophotometer was applied to performing qualitative and quantitative analysis of recovered solid products, and a wavelength range of 200-600 nm was selected. Clear and transparent plastics cuvettes were used for the measurements of TPA. Samples with varying strengths of terephthalic acid in the mass percentage range of 0.010wt% to 0.082wt% were made by dissolving terephthalic acid in 0.5 M NaOH solution, and the 0.5 NaOH solution was used as blank for the UV analysis. A calibration curve was determined by fitting the trend line between the UV absorbance and varying concentrations of standard terephthalic acid samples. The absorbance was controlled between 0.3-1.0 to ensure the accuracy of performing the quantitative determination of the end products in solid phase, terephthalic acid.

3.4.2 FT-IR analysis

Analysis of chemical functional groups was carried out by using Fourier transform-infrared spectroscopy (FT-IR). Both commercialized standard TPA and recovered TPA was characterized over a range of 4000-400 cm^{-1} by using a Spectrum Two FT-IR spectrophotometer (PerkinElmer, MA, USA). Similar to the FT-IR analysis of PET samples, around 10-30 mg TPA samples were placed onto the crystal surface. Later, commercial standard TPA and recovered TPA samples were pressed into the crystal head. Recovered TPA samples were obtained from PET hydrolyzed products.

3.4.3 TGA/ DTA analysis

Thermogravimetric analysis (TGA) was used for performing experiments for the terephthalic acid samples obtained from the degraded PET and the commercial standard terephthalic acid samples. TGA of commercialized standard recovered TPA samples were carried out under nitrogen gas by a Netzsch 209 F1 Libra TGA (NETZSCH Instruments, Burlington, MA) using an alumina pan. A

first-order differential thermogravimetric analysis (DTG) curve was obtained from the TGA curve. TGA and DTG analysis curves of commercial standard TPA and recovered TPA samples were compared.

3.4.4 HPLC analysis

Recovered end products obtained from the liquid phase were analyzed quantitatively and qualitatively by using High-Performance Liquid Chromatography (HPLC, Shimadzu LC-40) equipped with a RezexTM ROA-Organic Acid H+ (8%) column. A calibration curve was determined by fitting the trend line with measuring the composition of weight percent of standard ethylene glycol at 0.0024%-0.0414 wt%. 5 mM sulfuric acid was the mobile phase for this HPLC analysis, and the flow rate of the mobile phase was adjusted to 0.6 mL/min. The operation temperature for this HPLC column was set to 3°C. The signal was collected by using the refractive index (RID) at the wavelength of 284 nm.

Part 4 Results and Discussion

Ocean plastic waste, different from fresh plastics, experience environmental degradation processes, including radiation damage, mechanical stress, and oxidation. To some extent, environmental degradation in the ocean can affect the structural features and chemical properties of polymers. Ocean plastic waste belongs to a big family of waste plastics. Since the environmental degradation is complex, PET pretreated with various methods can be a good beginning to understand the structures and reactivity of ocean plastics.

The overall objective of this project was aiming at investigating the effect of mechanical stress and radiation damage on PET hydrolysis. Specific objectives were aiming at:

- 1) Reduce environmental contaminations resulted from ocean plastic waste contaminations.
- 2) Imitate environmental degradation in the ocean, including:
 - a. Perform high-energy ball-milling experiments to imitate the mechanical degradation in the ocean.
 - b. Perform photoaging experiments to imitate the radiation damage from the sunlight.
- 3) Study the effect of mechanical stress and radiation damage on structural features of PET, including the changes of crystallinity, chemical bonds, and morphology.
- 4) Investigate whether the changes of PET structures have effects on PET hydrolysis and compare the reactivity of virgin PET, photoaged PET and ball-milled PET, including:
 - a. Whether these treatments enhance the conversion rate of PET
 - b. Whether these treatments promote the yield of TPA

c. Whether these treatments facilitate the release of EG

Integrated results of the experiments are available in the **Appendix**. All the results and discussions are systematically divided:

(1) to study the structural features of untreated PET, ball-milled PET, and photoaged PET, including crystallinity, chemical bonds and morphology.

(2) to estimate the activation energy of PET neutral hydrolysis.

(3) to evaluate and compare the conversion rates and yields of end products of various PET feedstocks.

(4) to compare the reactivity between ball-milled PET and ball-milled cellulose and potential reasons for the difference in reactivity.

4.1 Structural features of pretreated PET

The initial aim of performing ball-milling and photoaging experiments was to study whether these pretreatments promote the conversion rate and chemical yields of main products. It was observed that the crystallization behavior and morphology of PET changed under ball-milling treatments. PET morphological patterns were also changed induced by photoaging experiments, while the photoaging treatment did not cause changes in chemical bonds. In this chapter, changes of crystallinity, chemical bonds, and morphology were discussed separately.

4.1.1. XRD data and crystallinity

The initial purpose of mechanical milling was to study the effect of de-crystallization of PET on the hydrolysis reaction of PET and the yield of products. Ball milling is a promising mechanical approach to de-crystallize PET. The PET specimens were ball-milled at different durations of time

in 12, 35, and 70 minutes separately. The XRD spectra of fresh PET and ball-milled PET were depicted in **Figure 17**. With the increased time of ball-milling, this treatment led to changes in structural features of PET.

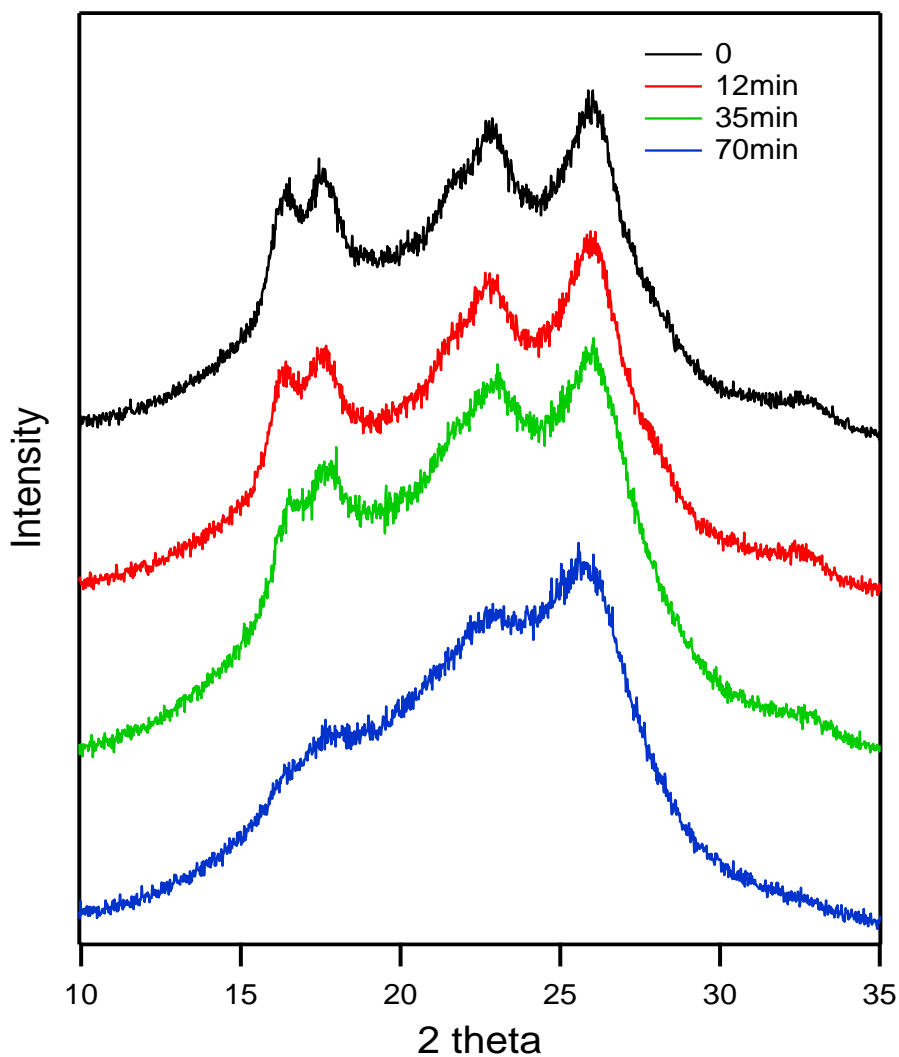


Figure 17 XRD diffractograms of progressively ball-milled PET samples: (a) blue: ball-milled PET after 70 min, (b) green: ball-milled PET after 35 min, (c) red: ball-milled PET after 12 min, (d) green: fresh PET.

The XRD diagram has indicated that ball-milling contributes to the decrease of the crystallinity of PET. To be more specific, the sharp peaks of untreated PET were clearly depicted. The

intensity of crystalline peaks decreased after aggressive ball-milling treatments. With longer ball-milling durations of time, the X-ray diffractogram has become broader and broader. After the 70-minute ball-milling treatments, the X-ray diffractogram of PET was nearly featureless. Several approaches have been proposed for estimating PET crystallinity using characterization methods, including (peak fitting, amorphous subtraction, and calculation).

The deconvolution of XRD spectra was divided into the area of amorphous halo and the total area of the crystalline bands, which has been shown in **Figure 18**. The wide amorphous halo was determined by the background produced by the amorphous phase. The apparent reflections crystal areas can be detected, and several intense crystal regions are characterized as the crystalline bands. The estimation and identification of the PET crystallinity are based on the quantitative analysis of amorphous halo and several crystalline bands.

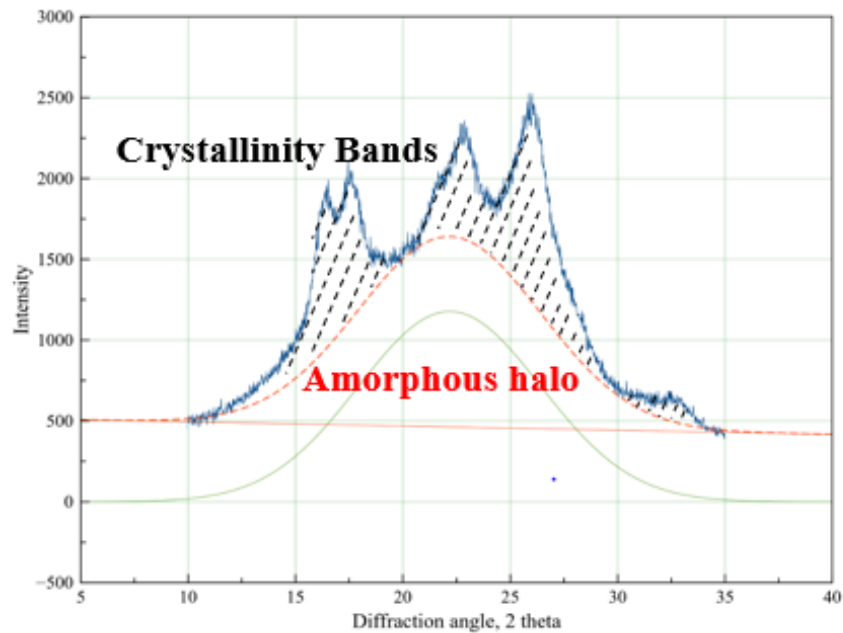


Figure 18 Devolution of XRD spectra for the estimation of PET crystallinity.

Deconvolution of spectrum and calculation of crystallinity were specified in equation (1) [46] to determine the effect of the mechanical treatment on crystallinity. **Figure 19** has shown the estimated PET crystallinity based on XRD spectra.

$$X_c = \frac{F - F_a}{F + k} \quad (1)$$

F – the normalized total area

F_a – the normalized area of the amorphous part of the XRD spectra for PET

k – the ratio of band intensities of 100% crystalline PET to amorphous PET for this study,

$k = 0.94$ [46]

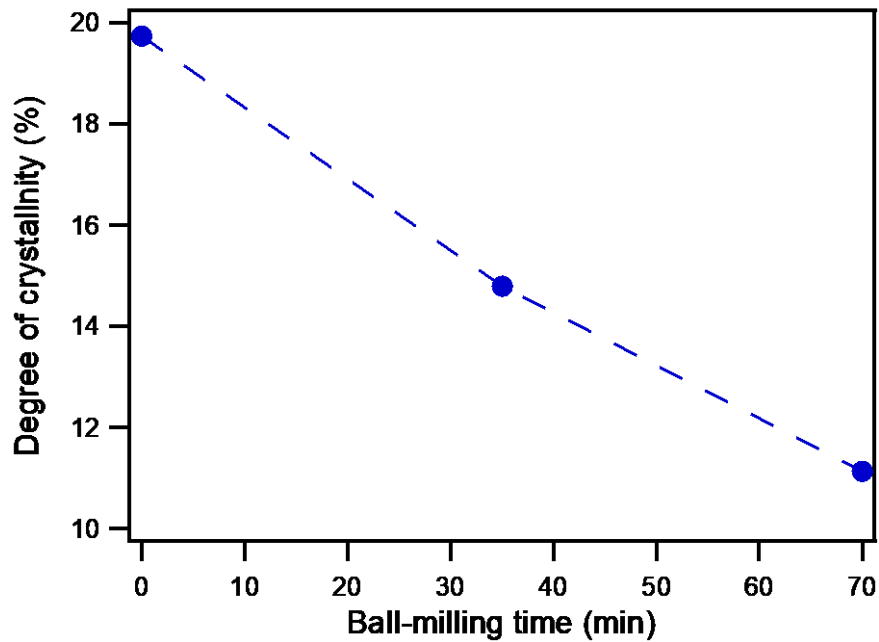


Figure 19 Degree of crystallinity for untreated PET samples, 35-min ball-milled PET samples and 70-min ball-milled PET samples.

4.1.2 Chemical-bond analysis: Raman microscopy and FT-IR

(Asmatulu et al., 2010) FT-IR and Raman analysis was applied to examine whether fractures of chemical bonds took place after the photoaging experiments, which determines the effect of the photo-damage on PET chemical properties. Characteristic absorption peaks of functional groups were analyzed separately in Raman spectra and FT-IR spectra, especially considering changes of C–C, C=C, C–O, and C=O bonds in PET.

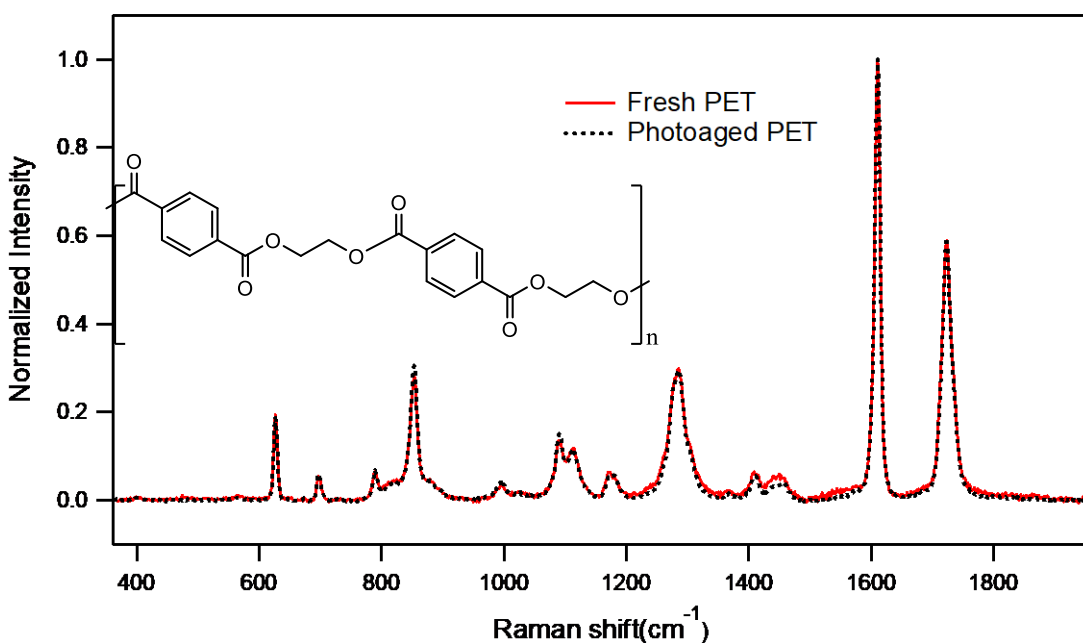


Figure 20 Raman spectra of fresh PET and photoaged PET.

Raman spectra of untreated PET and photoaged PET showed a high level of correlation in **Figure 20**. Raman peaks of chemical bonds in PET was interpreted in the following. Fundamentally, the C-C breathing (at around 860 cm⁻¹), C-C stretch, ring (at around 1425cm⁻¹), C=O stretch, ring (at around 1610cm⁻¹), and C=O stretch (at around 1720cm⁻¹) were observed in Raman spectra of untreated PET and photoaged PET. It indicated that these chemical bonds listed above did not change after the photoaging experiments.

FT-IR spectra of untreated PET and photoaged PET showed the similarities of the functional groups in **Figure 21**. Characteristic absorption peaks of functional groups of PET samples were interpreted in the following. In FT-IR spectra of untreated PET and photoaged PET, the C-H bending, ethyl (at around 735 cm^{-1}), C-O ester (at around 1120 and 1255 cm^{-1}), C-C phenyl ring (at around 1405 cm^{-1}) and C=O ester (at around 1725 cm^{-1}) were observed. It was discovered that chemical bonds listed above did not change after the photoaging experiments. This result support that the photoaging experiments did not lead to the generation of chemical bonds.

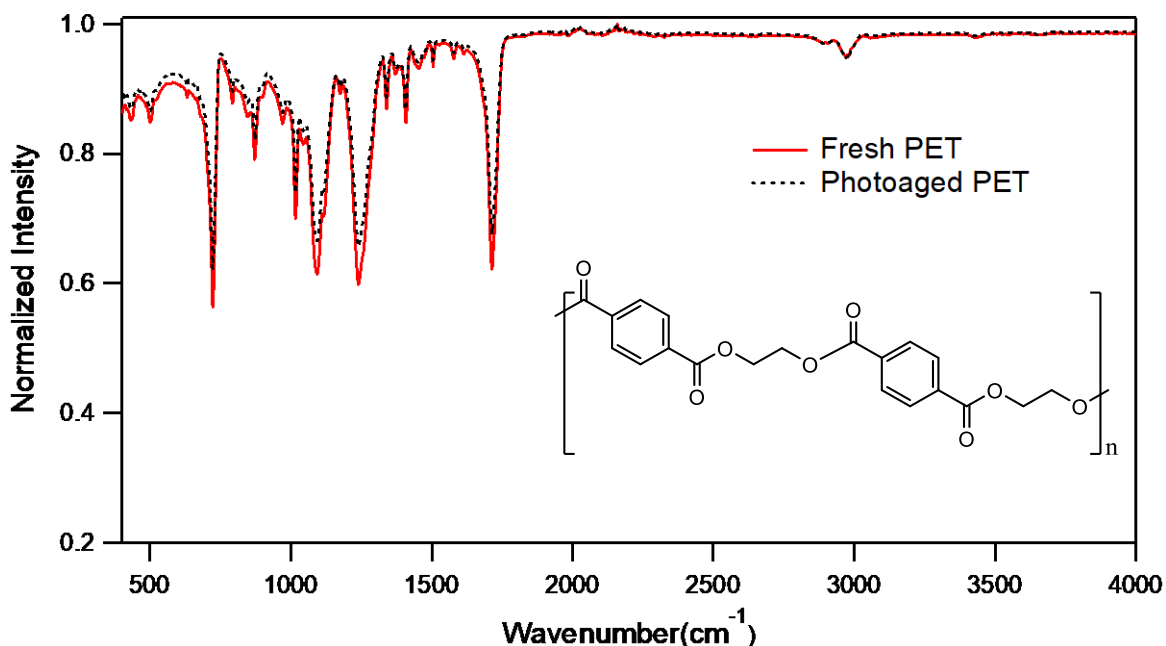


Figure 21 FT-IR spectra of fresh PET and photoaged PET.

In principle, photodegradation and fractures of chemical bonds could be occurred induced by the photoaging experiments, but the photoaging treatment in this experiment was not strong and long enough.

4.1.3 SEM and PET morphology

The effects of mechanical stress and radiation damage on the surface morphology of PET were observed by SEM. Images of SEM were conducted. The surfaces of image A (unpretreated PET), image B (ball-milled PET (12min)), image C (ball-milled PET (70min)), and image D (photoaged PET (after 12min ball-milling)) have been shown in **Figure 22**. Comparing image A to image C, the surface of the PET was fairly smooth after the 70-minute ball-milling treatment. Comparing image B with image D, the surface of photoaged PET was also smoother than the unpretreated PET. These results support that ball-milling and photoaging experiments led to changes in PET surface morphology.

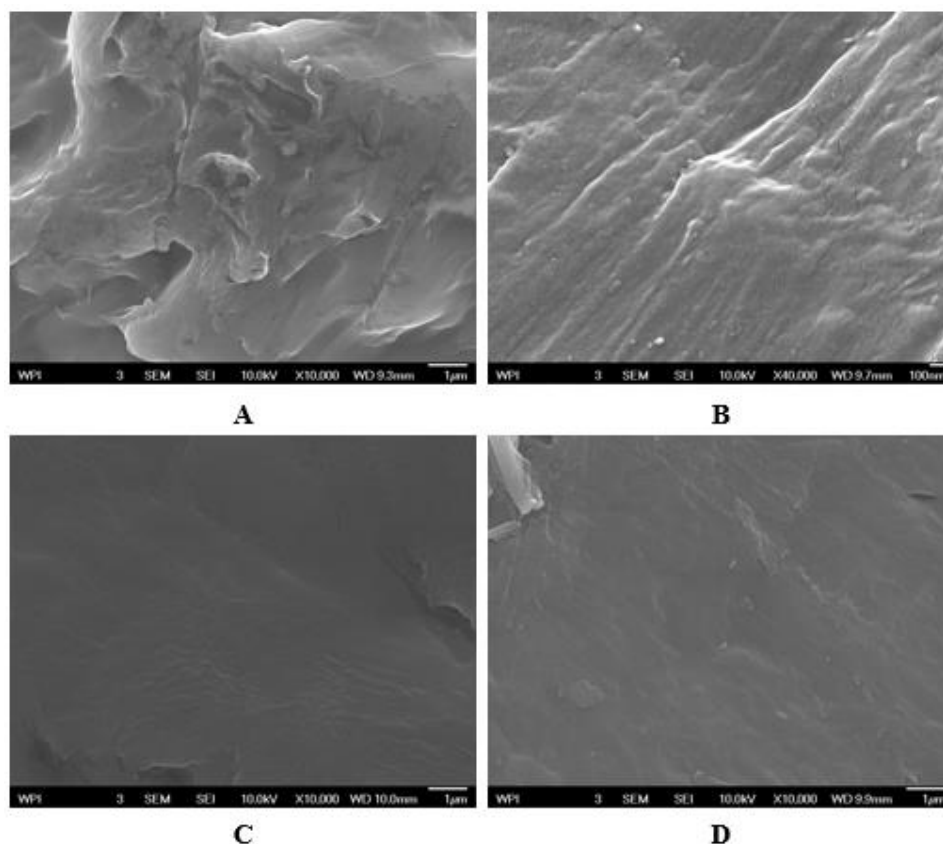


Figure 22 Scanning electron microscopy (SEM) images of sample: A (unpretreated PET), image B (ball-milled PET (12min)), image C (ball-milled PET (70min)), and image D (photoaged PET (after 12min ball-milling)).

Polyethylene terephthalate samples with various pretreatments were depolymerized in subcritical water at 200°C. After PET hydrolysis, terephthalic acid monomer and ethylene glycol monomer were generated, and there were certain amounts of oligomers and unreacted PET existing in the final products. Recovered TPA and EG exhibited similar patterns of standard TPA and EG in all the spectra or plots used in this experiment.

4.2.1 Characterization of Terephthalic Acid

4.2.1.1 TGA/DTG analysis of TPA

Terephthalic acid, the end solid product of PET hydrolysis, showed high level of correlations standard terephthalic acid in FT-IR spectra as well as curves of TGA and DTG (derivative thermogravimetric). All the results showed that the recovered TPA was highly purified.

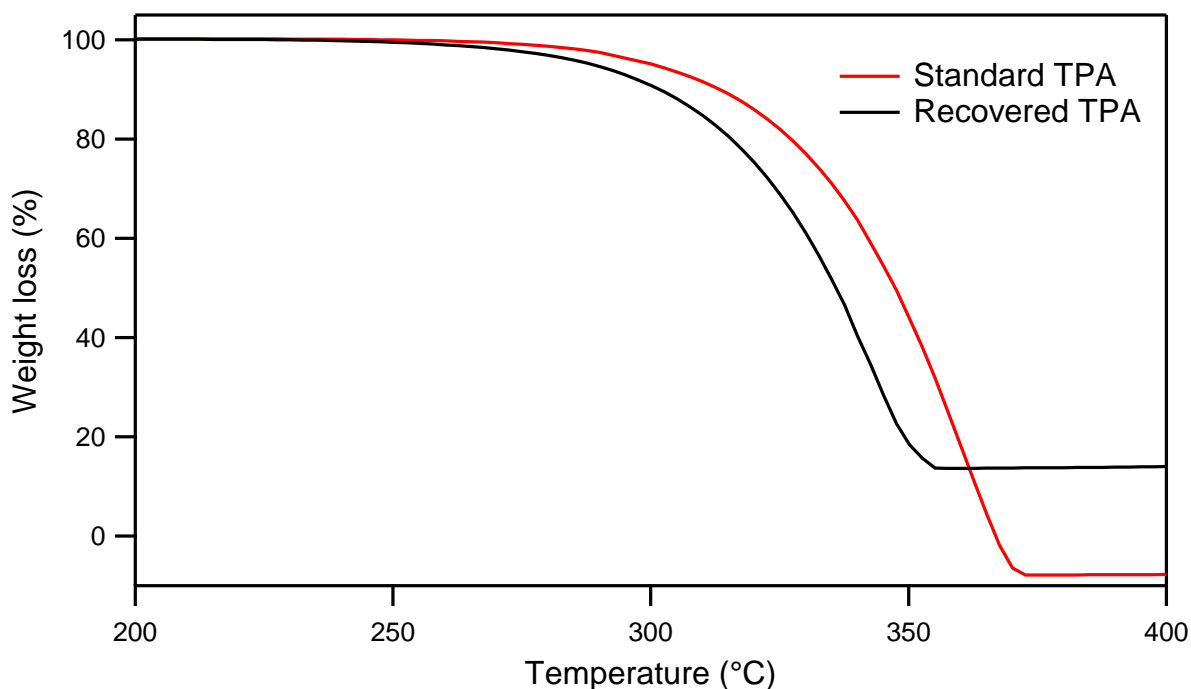


Figure 23 Thermogravimetric analysis (TGA) curves of recovered terephthalic acid (TPA) from hydrolyzed solid products and standard TPA.

TGA and DTG curves of recovered terephthalic acid from PET hydrolysis were similar to those curves of commercial standard terephthalic acid. TGA curves of recovered TPA and standard TPA were shown in **Figure 23**. Comparing the curve of standard TPA with that of recovered TPA obtained from PET hydrolysis, the weight loss of these two TGA curves followed similar trends. At around 250°C, both recovered and standard samples began to undergo thermal degradation. Approximately 50% of weight loss was observed over a range of temperatures between 320-300 °C. After 350 °C, all the TPA samples were rapidly degraded thermally. It was observed that the entire TPA samples were converted to vapor thoroughly at $365 \pm 10^\circ\text{C}$.

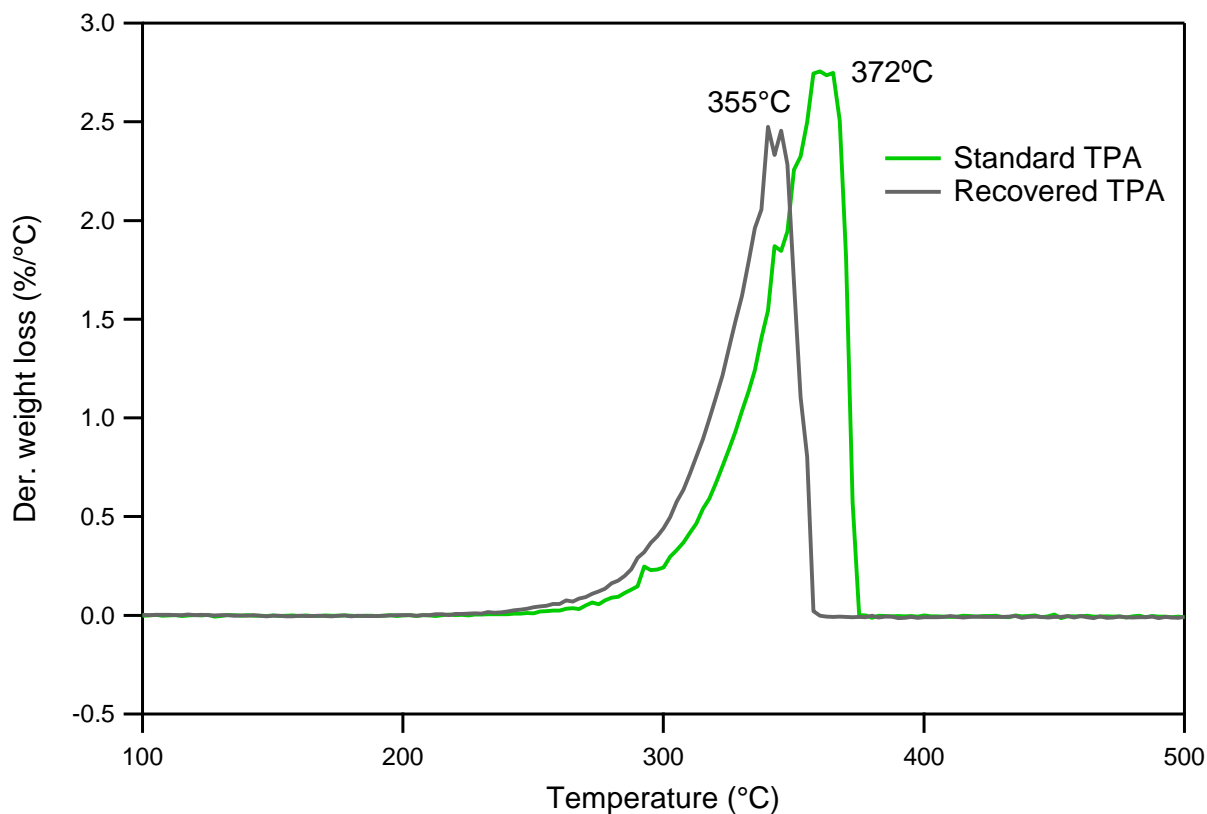


Figure 24 DTG (derivative thermogravimetric) curves of recovered TPA from hydrolyzed solid products and standard TPA.

DTG (derivative thermogravimetric) curves depicted in **Figure 24** were obtained by calculating the first derivative of TGA curves. DTG curves were plotted to determine helpful inflection points for in-depth explanations as well as thermogravimetric analysis. For standard and recovered terephthalic acid, the first derivatives of weight loss obtained from TGA curves followed similar trends. The major degradation peaks of standard TPA and recovered TPA appeared from the DTG plot to occur at around 355 and 372 °C respectively. These results from TGA and DTG curves clearly showed that the recovered TPA samples were pure. A small amount of impurities existed, which may indicate that some lighter organics may be carbonized while running TGA.

4.2.1.2 FT-IR analysis of TPA

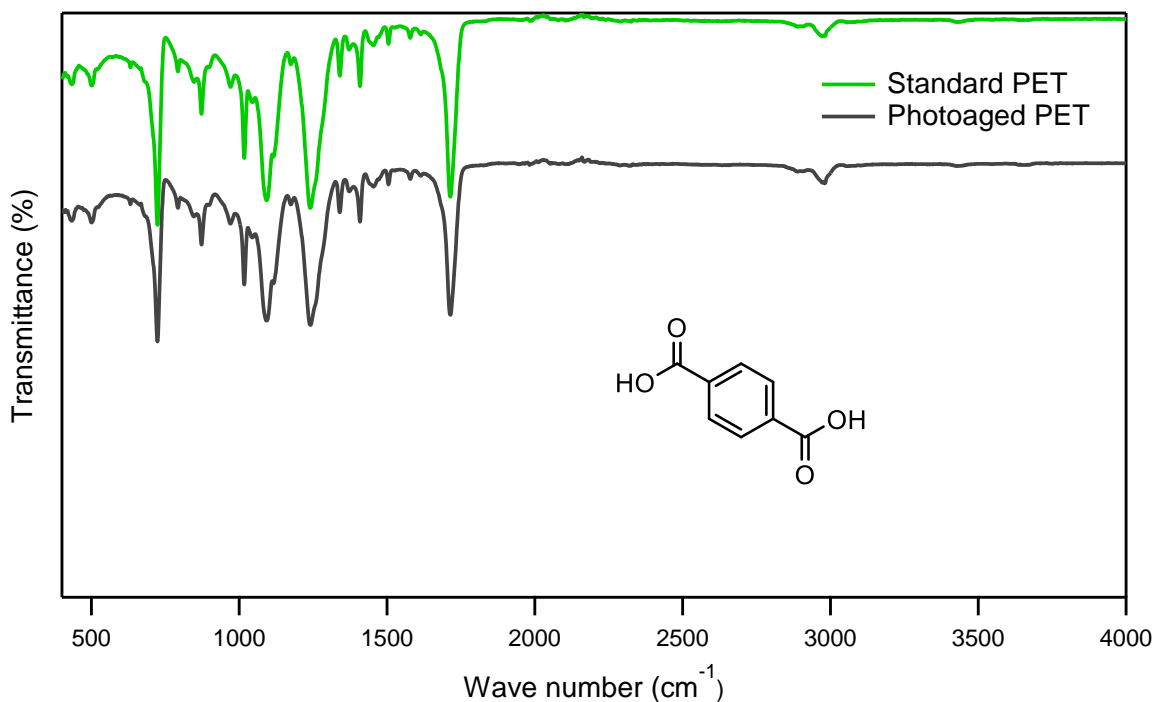


Figure 25 FT-IR spectra of recovered TPA from hydrolyzed solid products and standard TPA.

FT-IR spectra of recovered TPA and standard TPA showed the similarities of the functional groups in **Figure 25**. Also, it has directly shown a high level of correlations of FT-IR spectra for both

TPA samples. Characteristic absorption peaks of functional groups of TPA was interpreted in the following. Essentially, the C-O stretch in ester carbonyl (at around 1270cm^{-1}), C=C aromatic stretch (at around 1570cm^{-1}), and C=O stretch (at around 1720cm^{-1}) were observed in the FT-IR spectra of recovered and standard TPA. It strongly indicated that the terephthalic acid recovered from the solid products after PET hydrolysis was pure.

4.2.1.3 Quantitative analysis by UV-visible spectrophotometer

Terephthalic acid was analyzed qualitatively and quantitatively by using a UV-visible spectrophotometer. UV-visible curves of recovered TPA and standard TPA exhibited similar patterns in their spectra, which has been depicted in **Figure 26**.

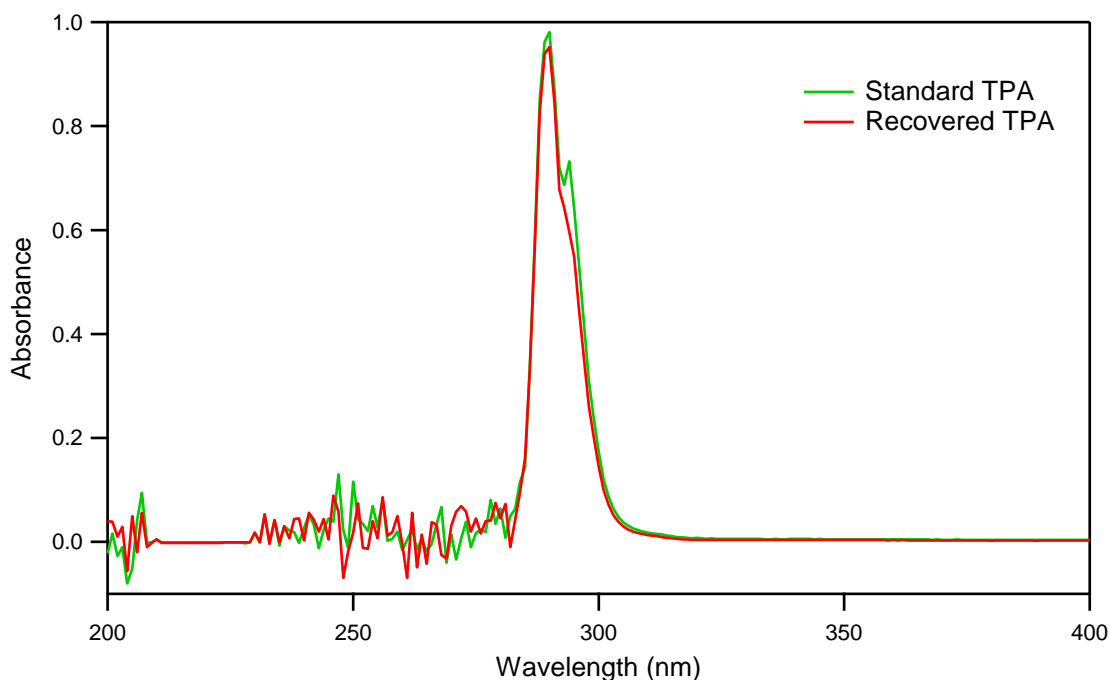


Figure 26. UV-visible curves of recovered TPA from hydrolyzed solid products and standard TPA.

The characteristic peak of recovered TPA was observed at 290 nm, which was the same as the characteristic peak of standard TPA. This result confirmed that the recovered TPA from

hydrolyzed solid products was indeed terephthalic acid. UV-Vis analysis was applied to quantify the amount of TPA obtained from PET hydrolysis. A linear-fit calibration curve of TPA standards with measuring the composition of weight percent of standard terephthalic acid was obtained, which has been shown in **Appendix A**. Yields of various TPA samples were calculated by using these weight percent values.

4.2.2 Characterization of Ethylene Glycol

Ethylene glycol, the end liquid product obtained from PET hydrolysis, was analyzed quantitatively by using High-Performance Liquid Chromatography. HPLC curves of standard and recovered EG showed a high level of correlation. It indicated that the recovered TPA was highly purified.

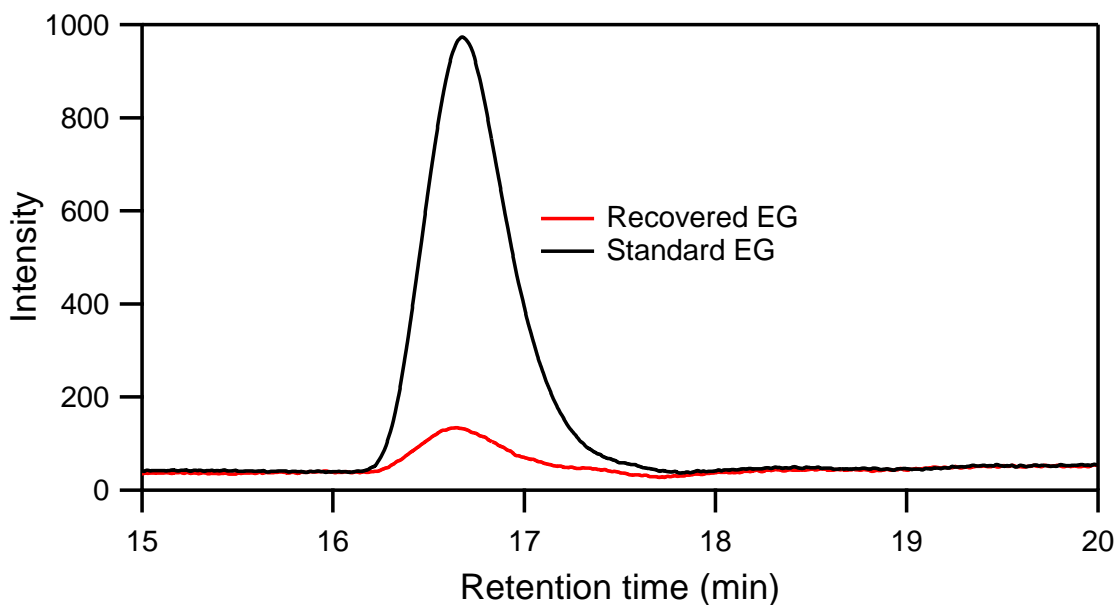


Figure 27 HPLC curves of recovered TPA from hydrolyzed solid products and standard TPA.

HPLC curves of recovered ethylene glycol were shown in **Figure 27**, which showed similarities of their characteristic peaks over a range of retention time 16 to 18 min. This result confirmed that the recovered EG from hydrolyzed liquid products was indeed ethylene glycol. Also, the amounts

of EG generated were measured by HPLC. A linear-fit calibration curve of EG standards with measuring the composition of weight percent of standard ethylene glycol was obtained, which has been shown in **Appendix A**. Yields of various EG samples were calculated by using these weight percent values.

4.3 Kinetic Analysis of PET hydrolysis

In this chapter, PET conversions were calculated by equation (2):

$$\begin{aligned}
 & \text{PET conversion (\%)} \\
 &= \frac{\text{weight of PET feedstock} - \text{weight of unreacted PET after reaction}}{\text{weight of PET feedstock}} \\
 & \times 100\% \quad (2)
 \end{aligned}$$

4.3.1 Condition selection based on PET conversions

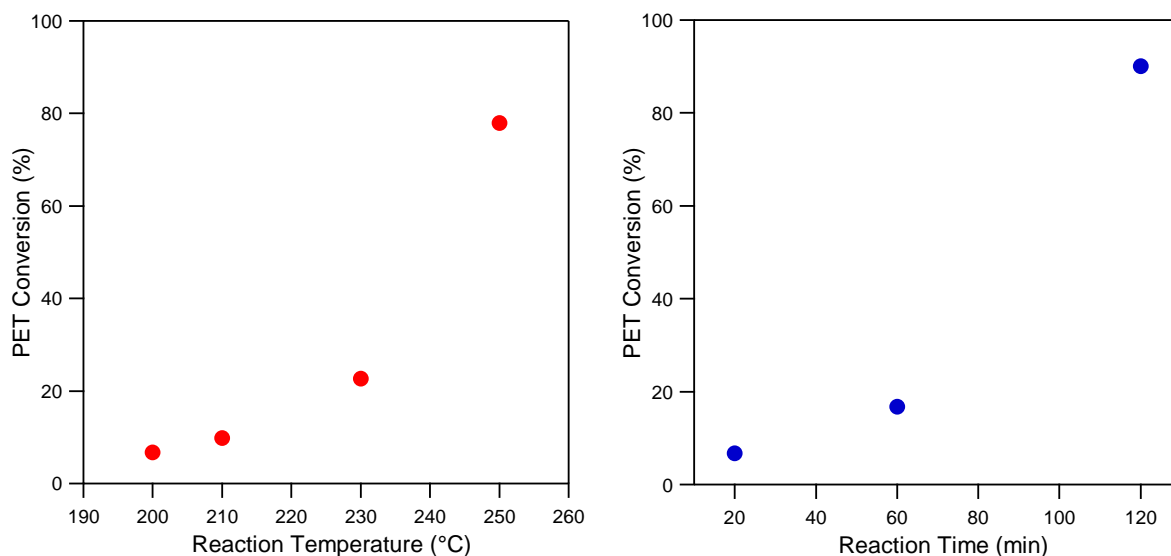


Figure 28 Depolymerization of PET at different reaction conditions: PET conversions at 20 min and different reaction temperatures; PET conversions at 200 °C and different retention times.

PET conversions at different reaction conditions were calculated by equation (2). On the left side of **Figure 28**, the red dots indicated that PET conversion increased with increasing temperature at

the 20 min. Above 230°C, PET conversions increased more rapidly than PET conversions at lower temperatures. On the right side of **Figure 28**, the blue dots indicated that PET conversions also improved with increasing retention time at 200°C. The optimized condition for this project should not be very high. The purpose is to study the effect of ball milling on the hydrolysis reactivity. The reaction temperature should be low enough. A condition that has a PET conversion between 10-20% should be selected, and the reaction condition (200°C/1hr) was selected for this study.

4.3.2 The activation energy of PET hydrolysis

Zope & Mishra (2008) have studied the reaction rate of PET neutral hydrolysis by measuring the concentration of PET waste at different retention times. It was determined experimentally that the reaction process of PET conversion was a first-order reaction. The first-order kinetics $R = k[PET]$ was applied for the kinetic analysis of PET depolymerization at subcritical water. Therefore, the first-order rate constant can be calculated by equation (3):

$$k = \frac{1}{t} \ln \frac{[PET]_o}{[PET]_t} \quad (3)$$

where, $[PET]_o$ represents the initial value of PET samples in gram. $[PET]_t$ represents the mass value of PET samples at the retention time, t [39].

Table 1 Kinetics of PET hydrolysis at different temperatures with the same retention time

Retention Time (s)	Reaction Temperature (°C)	PET conversion (%)	Rate constant k (s ⁻¹)
1200	200	6.745	5.82E-05
1200	210	9.805	8.59E-05
1200	230	22.680	2.14E-04
1200	250	77.965	1.26E-03

Estimating of the activation energy of PET hydrolysis is specified as follows. The rate constants at different temperatures were calculated by equation (3). The activation energy of PET hydrolysis can be obtained by applying the Arrhenius equation, which correlates the calculated rate constants and reaction temperatures. A linear equation arranged from the Arrhenius equation can be used for determining the activation energy by finding the slope of equation (4).

$$\ln(k) = -\frac{E_a}{R} \frac{1}{T} + \ln(A) \quad (4)$$

The following graph has shown activation energy is obtained by rearranging the Arrhenius equation. **Figure 29** represents $\ln(k)$ vs $1/T$ for a first-order reaction.

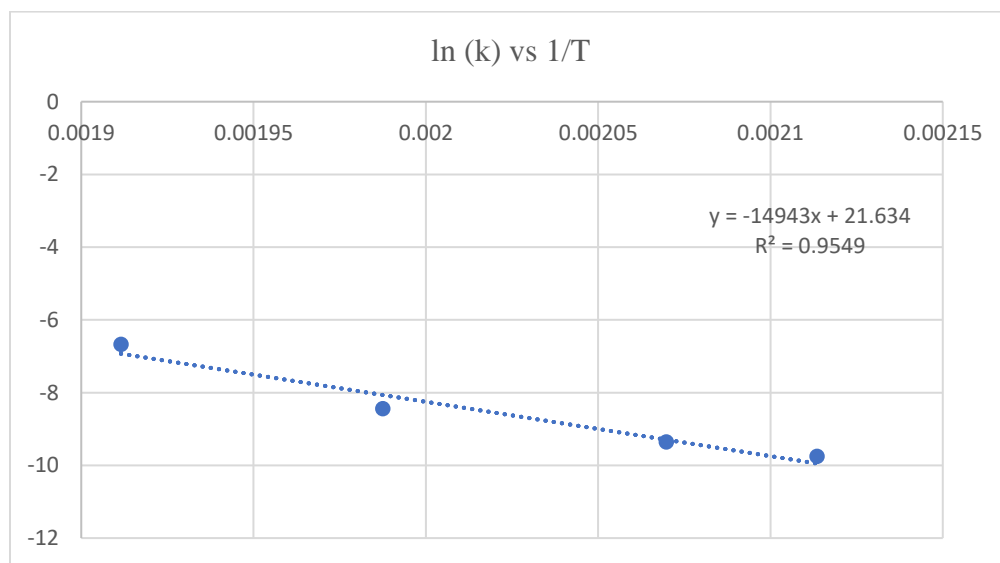


Figure 29 The rearranged linear equation of PET hydrolysis at subcritical water obtained from the Arrhenius equation

The activation energy is obtained by calculating equation (5), and the gas constant R equals to $8.314 \text{ J}\cdot\text{mol}^{-1}\cdot\text{K}^{-1}$ here.

$$-\frac{E_a}{R} = -14943 \quad (5)$$

$$E_a = 124236.1 \text{ J/mol} = 124 \text{ kJ/mol}$$

Therefore, the activation energy of PET hydrolysis is 124 kJ/mol at the reaction conditions in this study. In the previous studies, the activation energy for PET neutral hydrolysis was equal to about 90 [54] to 101 kJ/mol [55]. The activation energy in this study is higher than the previous results. Goje et al. (2004) performed PET hydrolysis in a batch reactor equipped with an agitator, ensuring that the feedstocks can be mixed well [54]. Since the calculation of activation energy was based on the calculated rate constants, different experimental operation conditions would affect the results potentially. For PET neutral hydrolysis, the reaction is catalyzed by hydrogen ions generated by the carboxyl end-groups [55]. The precipitation of TPA was thought to suppress the reaction rate of PET hydrolysis [56]. The micro-scale batch reactor in this study did not equipped with an agitator. The reaction should be slower, and the TPA precipitated on PET cores would decrease the reaction rate, so calculated rate constants were smaller. Therefore, the larger activation energy value is owing to the lower rate constant values. However, with the existence of the potassium hydroxide solution, the activation energy of PET alkaline hydrolysis was only 69 kJ/mol [57]. Compared to neutral hydrolysis, the hydrolysis can be faster at the same reaction condition. The use of catalysts should be considered in future work.

4.4 Conversion rates and product yields of PET hydrolysis

It was confirmed that ball-milling and photoaging experiments can have effects on PET structures. It was mainly discussed whether these treatments can affect PET reactivity in this chapter. As the reaction time and temperature increasing, conversion rates and product yields were all improved. The depolymerization behaviors under various reaction conditions were observed. In this chapter,

effects of mechanical stress and radiation damage were studied at 1-hour and 2-hour reaction time.

In this chapter, all the results were calculated by equation (2), equation (5), and equation (6):

$$\begin{aligned} \text{TPA yield (\%)} &= \frac{\text{weight of TPA generated}}{\text{estimated weight of TPA for fully depolymerization of PET}} \\ &\times 100\% \quad (5) \end{aligned}$$

$$\begin{aligned} \text{EG yield (\%)} &= \frac{\text{weight of EG produced}}{\text{estimated weight of EG for fully depolymerization of PET}} \\ &\times 100\% \quad (6) \end{aligned}$$

4.4.1 Evaluation of PET reactivity after ball-milling treatment

PET was depolymerized into ethylene glycol and terephthalic acid at hot compressed water. PET conversion, EG yield and TPA yield were obtained for evaluating the reactivity of various PET feedstocks. The conversion rate and yields of end products were treated at 200°C.

The depolymerization behaviors of fresh PET and ball-milled were observed at various durations of reaction time, which has been shown in **Figure 28**. The conversion rate of PET and yields of end products were as a function of retention time. The conversion rate of all PET samples was around 16 – 18% after 1 hour, and it reached around 87-91% after 2 hours. In general, the yield of EG was much lower than the yield of TPA. After a one-hour retention time, the yields of TPA and EG were $11 \pm 1\%$ and $0.7 \pm 0.1\%$ respectively. After a two-hour retention time, the yields of end products improved dramatically, and the yields of TPA and EG were $88 \pm 1.5\%$ and $9.5 \pm 0.7\%$ separately. This depolymerization behavior strongly supported that the conversion rate of PET and yields of end products improved with increasing reaction time at the same temperature.

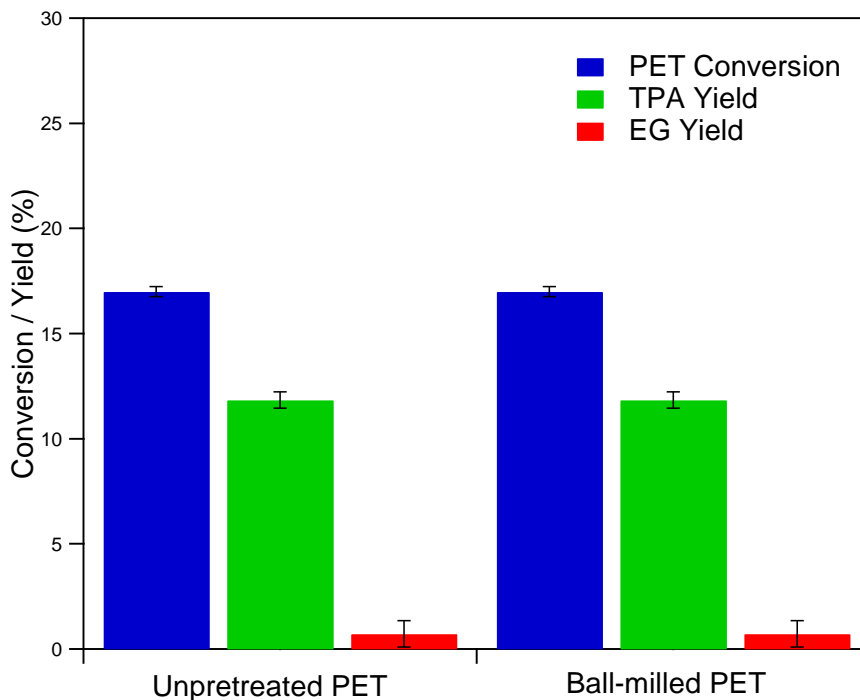


Figure 30 PET conversion rate, TPA yield and EG yield of unpretreated PET samples and ball-milled PET samples (70min) after a reaction time of 1 hour.

Reactivity of fresh PET and ball-milled PET were compared at 200°C across two different reaction times of 1 hour and 2 hours. Both the conversion rate and the yields of end products were very similar. Although the structural properties of PET changed after ball-milling treatments, the reactivity did not vary a lot. Conversion of PET and yield of TPA were not improved after ball-milling. The release of ethylene glycol was not facilitated after ball-milling. Ball-milling experiments may affect the reactivity of PET. However, the transition temperature of PET was 81°C [42], which was much lower than the reaction temperature in this experiment. The structure of PET had already changed when the reaction took place at 200 °C. Reaction temperature plays a more dominant role compared to PET structural features at this reaction condition.

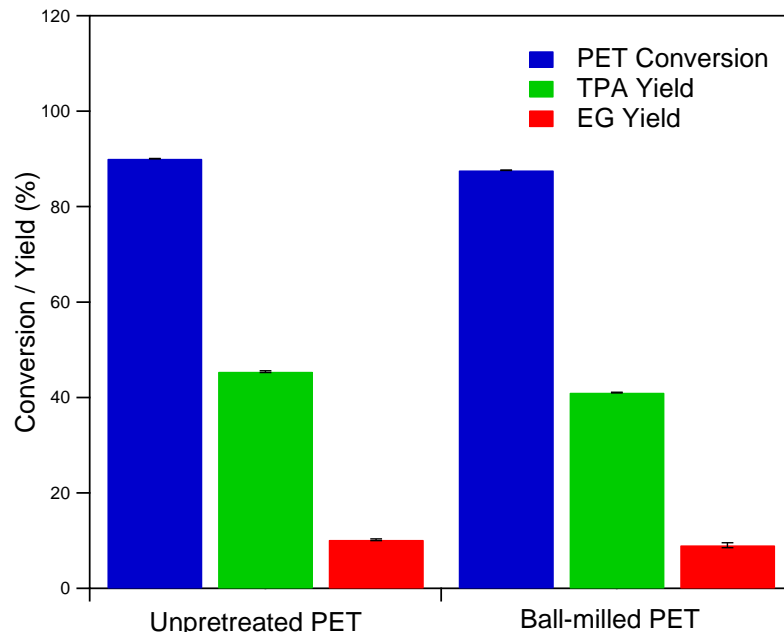


Figure 31 PET conversion rate, TPA yield and EG yield of unpretreated PET samples and ball-milled PET samples (70min) after a reaction time of 2 hour.

4.4.2 Comparisons of PET and cellulose reactivity after ball-milling

Cellulose, another type of polymer, can be hydrolyzed to generate fuels and chemicals. Ball-milling treatments successfully decreased its crystallinity, and the effect of mechanical treatment on cellulose reactivity was confirmed. Mechanical milling increased its hydrolysis reactivity. The ball-milled cellulose samples were hydrolyzed in an acidic environment at 150°C [30]. The glass transition temperature of cellulose was up to 180°C [58]. At the reaction temperature of 150 °C, the structure of cellulose did not vary dramatically. The effect of ball-milling treatment on cellulose reactivity can be exhibited. By contrast, the reaction temperature of PET hydrolysis in this experiment was much higher than the transition temperature of PET. Therefore, temperature may affect the results regardless of the mechanical treatment on PET reactivity. Considering the future outlook of this studying mechanical effect on PET reactivity, PET hydrolysis should be performed at lower temperatures under the action of catalysts.

4.4.3 Evaluation of PET reactivity after photoaging treatment

Photoaged PET samples were also depolymerized into ethylene glycol and terephthalic acid in subcritical water. The PET conversion, yield of EG, and yield of TPA of untreated PET and photoaged PET were compared for evaluating the reactivity of photoaged PET. The conversion rate and yields of end products were treated at 200°C with the retention time of 1 hour.

The depolymerization behavior of photoaged PET was observed at 200°C after 1 hour, which has been depicted in **Figure 30**. The conversion rate of photoaged PET samples was around $16.5 \pm 0.5\%$ after 1 hour. Accordingly, the yield of EG was also much lower than the yield of TPA. After 1 hour of retention time, the yields of TPA and EG were $10 \pm 1\%$ and $0.9 \pm 0.2\%$ separately. Reactivity of fresh PET and ball-milled PET were studied at 200°C by comparing their product yields and conversion rates. Both the conversion rate and the yield of end products were very similar.

The morphology and chemical bonds of PET changed after photo-damaging treatment. However, the reactivity of fresh PET and photoaged PET was quite similar. The photoaging treatment had nothing to do with increasing conversion rate, improving the yield of TPA, and facilitating the release of ethylene glycol.

There are two main reasons to explain this phenomenon. Same as the HTL experiment of ball-milled PET, the structure of photoaged PET had already changed before the reaction took place. The effect of radiation damage was obscured by the more effective reaction condition, temperature. Another possible reason is that the photoaging treatment in this experiment was not enough to result in a dramatic change in PET reactivity. Ultraviolet light can do damage to the mechanical and chemical properties of polymers [29]. The radiation damage treatment of this experiment was only equal to 96-hour natural sunlight in the Gulf of Mexico [53]. Therefore, this treatment was

not strong enough to affect PET reactivity. Longer durations of photo-damaging treatment are needed to be done in the future.

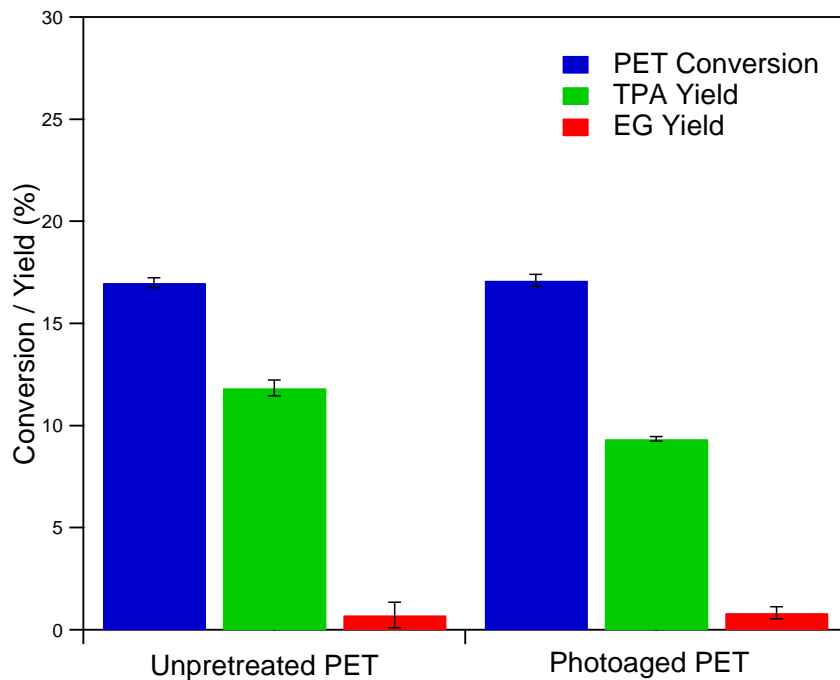


Figure 32 PET conversion rate, TPA yield and EG yield of unpretreated PET samples and photoaged ET samples (70min) after a reaction time of 1 hour.

Part 5 Conclusions

In summary, this study was aiming at investigating the effect of mechanical stress and radiation damage on the physical and chemical properties of PET. To explore the effects of mechanical stress on PET reactivity, mechanical de-crystallization on PET hydrolysis was investigated. It was confirmed that ball-milling treatments decreased PET crystallinity. However, ball milling did not increase PET reactivity. The transition temperature of PET was much lower than the reaction temperature in this experiment, so the effects of mechanical stress on PET reactivity could not be perceived. PET conversion rate and yields of end products (EG and TPA) were improved dramatically after 2 hours. It indicated that the conversion of PET and yields of end products improved with increasing reaction time. To examine the effects of radiation damage on PET reactivity, chemical properties of PET were investigated after photodegradation. The photoaging treatment was not strong enough owing to the short treatment time and weak ultraviolet light intensity. PET structures did not vary a lot, and PET reactivity did not increase. These results confirmed that mechanical stress and radiation damage did have effects on PET physical and mechanical properties. The effects on PET reactivity should be further studied.

Part 6 Future Outlooks

6.1 Recommendations for improved analytical techniques

6.1.1 Analysis of chemical modifications induced by UV laser

Changes of chemical properties induced by solar light or UV laser can be inspected via micro-Raman spectroscopy and fluorescence spectroscopy. Rebollar et al. (2014) have discovered that the fluorescence background of irradiated PET increased compared to untreated PET samples. Rearrangements of polymer chains and the appearance of new carboxylic groups were observed by using micro-Raman analysis [59]. In future work, these two spectral analytical techniques would permit to understand changes of chemical properties after solar light damage or UV laser damage treatments.

6.1.2 Surface chemistry study of PET samples

In this study, SEM analysis can provide information on morphological changes after the ball milling and photoaging treatments, but the changes in surface energy were unknown. To understand the effect of surface changes on reactivity, surface energy analysis can be helpful. El-Saftawy et al. (2014) studied the surface changes after electron beam irradiation. Atomic force microscope (AFM) analysis revealed changes of surface roughness and surface free energy after electrons–PET surface interactions [60]. As a result of radical forming on the surface of PET after photoaging or ball milling, changes of surface energy could also be observed by the Atomic force microscope (AFM). Further analysis of surface chemistry can allow to study the physical properties of PET surface and its hydrolysis reactivity.

6.1.3 Molecular weight evaluations

Ball milling treatment can lead to a decrease of averaged molecular weight. To study the effect of mechanical stress on PET hydrolysis reactivity, evaluations of PET molecular weight can provide more explanations. Sanches, Dias, and Pacheco (2005) developed comparative techniques for evaluating the molecular weight of PET samples. Performing size exclusive chromatography (SEC) analysis in hexafluoroisopropanol with PMMA standards allowed the determination of averaged molecular weight of PET samples [61].

6.2 Directions for PET hydrolysis study

6.2.1 Improved experimental procedures for the future study

First, the reaction condition of PET hydrolysis should be changed and further studied. Based on current results, ball-milling and photoaging pretreatments did not increase PET reactivity. Reaction temperatures should be lower to prevent PET from melting before the reaction takes place. It is challenging to perform PET hydrolysis lower than its transition temperature, 81°C [42]. However, it was elaborated in the **background** that hydrolysis with acids, bases, or catalysts can increase PET reactivity. With the existence of catalysts, PET hydrolysis can be carried out at lower temperatures. It would be much easier to study the effects of de-crystallization on reactivity. With the existence of sulfuric acid, PET hydrolysis can take place at 150°C, which allowed to perform PET hydrolysis at lower temperatures [62].

Second, stronger radiation damage pretreatments should be applied, which can result in more dramatic structural changes in PET. It is evident that improving pretreatment time can be helpful. More experiments can be carried out, including using natural light and ultraviolet light to photodegrade PET. PET reactivity can be evaluated and compared after this new photodamaging treatment method.

6.2.2 Future work for improving ethylene glycol yield

The lower yield of ethylene glycol was due to its dihydroxylation to aldehyde and polymerization to diethylene glycols catalyzed by TPA [21]. Performing alkaline hydrolysis may increase the yield of ethylene glycol since it can avoid the proton effects on PET hydrolysis with the existence of terephthalic acid. PET can be hydrolyzed at dilute aqueous ammonia solution [63]. It was also discovered that the amounts of ethylene glycol increased with the existence of potassium hydroxide, while sodium hydroxide did not have this effect [64]. The ethylene glycol stability studies and PET alkaline hydrolysis experiments can be done in the future to obtain an optimized condition with higher EG yields. PET alkaline hydrolysis can be performed in a series of KOH or aqueous ammonia solutions with different concentrations. The yields of EG can be compared to find a condition with maximum ethylene glycol yield.

Part 7 References

1. Forbid, G.T., et al., *Open waste burning in Cameroonian cities: an environmental impact analysis*. The Environmentalist, 2011. **31**(3): p. 254-262.
2. Jambeck, J.R., et al., *Plastic waste inputs from land into the ocean*. Science, 2015. **347**(6223): p. 768-771.
3. Al-Maadad, M., et al., *An overview of solid waste management and plastic recycling in Qatar*. Journal of Polymers and the Environment, 2012. **20**(1): p. 186-194.
4. Troschinetz, A.M. and J.R. Mihelcic, *Sustainable recycling of municipal solid waste in developing countries*. Waste management, 2009. **29**(2): p. 915-923.
5. Kaza, S., et al., *What a waste 2.0: a global snapshot of solid waste management to 2050*. 2018: The World Bank.
6. Marshall, R.E. and K. Farahbakhsh, *Systems approaches to integrated solid waste management in developing countries*. Waste management, 2013. **33**(4): p. 988-1003.
7. Kadir, S.A.S.A., et al., *Incineration of municipal solid waste in Malaysia: Salient issues, policies and waste-to-energy initiatives*. Renewable and Sustainable Energy Reviews, 2013. **24**: p. 181-186.
8. Beede, D.N. and D.E. Bloom, *The economics of municipal solid waste*. The World Bank Research Observer, 1995. **10**(2): p. 113-150.
9. Agarwal, A., et al., *Municipal solid waste recycling and associated markets in Delhi, India*. Resources, Conservation and Recycling, 2005. **44**(1): p. 73-90.
10. Subramanian, P., *Plastics recycling and waste management in the US*. Resources, Conservation and Recycling, 2000. **28**(3-4): p. 253-263.

11. Gregory, M.R., *Plastics and South Pacific Island shores: environmental implications*. Ocean & Coastal Management, 1999. **42**(6-7): p. 603-615.
12. Kershaw, P., et al., *Plastic debris in the ocean*. 2011, United Nations Environment Programme.
13. Laist, D.W., *Overview of the biological effects of lost and discarded plastic debris in the marine environment*. Marine pollution bulletin, 1987. **18**(6): p. 319-326.
14. LI, W.C., H. Tse, and L. Fok, *Plastic waste in the marine environment: A review of sources, occurrence and effects*. Science of the Total Environment, 2016. **566**: p. 333-349.
15. Ritchie, H. and M. Roser, *Plastic pollution*. Our World in Data, 2018.
16. Shelley, S., *Plastics reborn*. Chemical Engineering, 1992. **99**(7): p. 30.
17. He, W., et al., *Application of hydrothermal reaction in resource recovery of organic wastes*. Resources, Conservation and Recycling, 2008. **52**(5): p. 691-699.
18. Dimitriadis, A. and S. Bezergianni, *Hydrothermal liquefaction of various biomass and waste feedstocks for biocrude production: A state of the art review*. Renewable and Sustainable Energy Reviews, 2017. **68**: p. 113-125.
19. Gu, L. and T. Ozbakkaloglu, *Use of recycled plastics in concrete: A critical review*. Waste Management, 2016. **51**: p. 19-42.
20. Goto, M., *Chemical recycling of plastics using sub-and supercritical fluids*. The Journal of Supercritical Fluids, 2009. **47**(3): p. 500-507.
21. Sato, O., K. Arai, and M. Shirai, *Hydrolysis of poly (ethylene terephthalate) and poly (ethylene 2, 6-naphthalene dicarboxylate) using water at high temperature: Effect of proton on low ethylene glycol yield*. Catalysis Today, 2006. **111**(3-4): p. 297-301.

22. Sinha, V., M.R. Patel, and J.V. Patel, *PET waste management by chemical recycling: a review*. Journal of Polymers and the Environment, 2010. **18**(1): p. 8-25.
23. Achilias, D. and G. Karayannidis, *The chemical recycling of PET in the framework of sustainable development*. Water, air and soil pollution: Focus, 2004. **4**(4-5): p. 385-396.
24. Carta, D., G. Cao, and C. D'Angeli, *Chemical recycling of poly (ethylene terephthalate)(PET) by hydrolysis and glycolysis*. Environmental Science and Pollution Research, 2003. **10**(6): p. 390-394.
25. Karayannidis, G., A. Chatziavgoustis, and D. Achilias, *Poly (ethylene terephthalate) recycling and recovery of pure terephthalic acid by alkaline hydrolysis*. Advances in Polymer Technology: Journal of the Polymer Processing Institute, 2002. **21**(4): p. 250-259.
26. Paszun, D. and T. Szychaj, *Chemical recycling of poly (ethylene terephthalate)*. Industrial & engineering chemistry research, 1997. **36**(4): p. 1373-1383.
27. Bai, C., et al., *Structural changes in poly (ethylene terephthalate) induced by mechanical milling*. Polymer, 2000. **41**(19): p. 7147-7157.
28. Boyer, R.F., *Mechanical motions in amorphous and semi-crystalline polymers*. Polymer, 1976. **17**(11): p. 996-1008.
29. Ghasemi-Kahrizsangi, A., et al., *Improving the UV degradation resistance of epoxy coatings using modified carbon black nanoparticles*. Progress in Organic Coatings, 2015. **85**: p. 199-207.
30. Tyufekchiev, M., et al., *Reaction engineering implications of cellulose crystallinity and water-promoted recrystallization*. Green Chemistry, 2019. **21**(20): p. 5541-5555.

31. Michalski, A., *Hydrolysis of Poly (ethylene terephthalate) Waste to Obtain Terephthalic Acid*. *WI. Chem*, 1987. **49**: p. 144.
32. Van Willige, R., et al., *Influence of flavour absorption by food-packaging materials (low-density polyethylene, polycarbonate and polyethylene terephthalate) on taste perception of a model solution and orange juice*. *Food Additives & Contaminants*, 2003. **20**(1): p. 84-91.
33. Heinze, H. and E. Hackel, *Process for making linear polyesters from ethylene glycol and terephthalic acid*. 1978, Google Patents.
34. Yue, H., et al., *Ethylene glycol: properties, synthesis, and applications*. *Chemical Society Reviews*, 2012. **41**(11): p. 4218-4244.
35. Adschiri, T., et al., *Recovery of terephthalic acid by decomposition of PET in supercritical water*. *Kagaku Kogaku Ronbunshu*, 1997. **23**(4): p. 505-511.
36. Oku, A., L.C. Hu, and E. Yamada, *Alkali decomposition of poly (ethylene terephthalate) with sodium hydroxide in nonaqueous ethylene glycol: a study on recycling of terephthalic acid and ethylene glycol*. *Journal of Applied Polymer Science*, 1997. **63**(5): p. 595-601.
37. Yoshioka, T., T. Motoki, and A. Okuwaki, *Kinetics of hydrolysis of poly (ethylene terephthalate) powder in sulfuric acid by a modified shrinking-core model*. *Industrial & engineering chemistry research*, 2001. **40**(1): p. 75-79.
38. Liu, Y., M. Wang, and Z. Pan, *Catalytic depolymerization of polyethylene terephthalate in hot compressed water*. *The Journal of Supercritical Fluids*, 2012. **62**: p. 226-231.

39. Zope, V.S. and S. Mishra, *Kinetics of neutral hydrolytic depolymerization of PET (polyethylene terephthalate) waste at higher temperature and autogenous pressures*. Journal of applied polymer science, 2008. **110**(4): p. 2179-2183.
40. Daraei, P., et al., *Novel polyethersulfone nanocomposite membrane prepared by PANI/Fe₃O₄ nanoparticles with enhanced performance for Cu (II) removal from water*. Journal of Membrane Science, 2012. **415**: p. 250-259.
41. Meijer, H.E. and L.E. Govaert, *Mechanical performance of polymer systems: The relation between structure and properties*. Progress in polymer science, 2005. **30**(8-9): p. 915-938.
42. Demirel, B., A. Yaraş, and H. Elçiçek, *Crystallization behavior of PET materials*. 2011.
43. Jones, R.A.L., *Polymers at surfaces and interfaces*. 1999: Cambridge University Press.
44. Bhat, N. and R. Deshmukh, *X-ray crystallographic studies of polymeric materials*. 2002.
45. Mandelkern, L., *The relation between structure and properties of crystalline polymers*. Polymer Journal, 1985. **17**(1): p. 337-350.
46. Gruver, V., et al. *The Determination of PET Crystallinity by Different Analytical Techniques (879)*. in *TECHNICAL PAPERS OF THE ANNUAL TECHNICAL CONFERENCE-SOCIETY OF PLASTICS ENGINEERS INCORPORATED*. 2000.
47. Fachine, G., R. Souto-Maior, and M. Rabello, *Structural changes during photodegradation of poly (ethylene terephthalate)*. Journal of materials science, 2002. **37**(23): p. 4979-4984.
48. Fachine, G., et al., *Surface characterization of photodegraded poly (ethylene terephthalate). The effect of ultraviolet absorbers*. Polymer, 2004. **45**(7): p. 2303-2308.

49. Asmatulu, R., et al. *Effects of UV light on water contact angles of nanocomposite coatings*. in *Proceedings of the SAMPE Fall Technical Conference, Salt Lake City, UT, USA*. 2010.
50. Nikafshar, S., et al., *The effects of UV light on the chemical and mechanical properties of a transparent epoxy-diamine system in the presence of an organic UV absorber*. *Materials*, 2017. **10**(2): p. 180.
51. Harper, J.J. and P. Janik, *Terephthalic acid solubility*. *Journal of Chemical and Engineering Data*, 1970. **15**(3): p. 439-440.
52. Ravichandran, S.A., et al. *Characterization of Terephthalic Acid Monomer Recycled from Post-Consumer PET Polymer Bottles*. in *Macromolecular Symposia*. 2016. Wiley Online Library.
53. Zito, P., et al., *Molecular-Level Composition and Acute Toxicity of Photosolubilized Petrogenic Carbon*. *Environmental science & technology*, 2019. **53**(14): p. 8235-8243.
54. Goje, A., et al., *Hydrolytic depolymerization of poly (ethylene terephthalate) waste at high temperature under autogenous pressure*. *Polymer-Plastics Technology and Engineering*, 2004. **43**(4): p. 1093-1113.
55. Ravens, D. and I. Ward, *Chemical reactivity of polyethylene terephthalate. Hydrolysis and esterification reactions in the solid phase*. *Transactions of the Faraday Society*, 1961. **57**: p. 150-159.
56. Yoshioka, T., N. Okayama, and A. Okuwaki, *Kinetics of hydrolysis of PET powder in nitric acid by a modified shrinking-core model*. *Industrial & engineering chemistry research*, 1998. **37**(2): p. 336-340.

57. Wan, B.-Z., C.-Y. Kao, and W.-H. Cheng, *Kinetics of depolymerization of poly (ethylene terephthalate) in a potassium hydroxide solution*. Industrial & engineering chemistry research, 2001. **40**(2): p. 509-514.
58. Szcześniak, L., A. Rachocki, and J. Tritt-Goc, *Glass transition temperature and thermal decomposition of cellulose powder*. Cellulose, 2008. **15**(3): p. 445-451.
59. Rebollar, E., et al., *Physicochemical modifications accompanying UV laser induced surface structures on poly (ethylene terephthalate) and their effect on adhesion of mesenchymal cells*. Physical Chemistry Chemical Physics, 2014. **16**(33): p. 17551-17559.
60. El-Saftawy, A., et al., *Electron beam induced surface modifications of PET film*. Radiation Physics and Chemistry, 2014. **102**: p. 96-102.
61. Sanches, N., M. Dias, and E. Pacheco, *Comparative techniques for molecular weight evaluation of poly (ethylene terephthalate)(PET)*. Polymer testing, 2005. **24**(6): p. 688-693.
62. Mehrabzadeh, M., S. Shodjaei, and M. Khosravi, *Chemical recycling of polyethylene terephthalate*. 2000.
63. Zenda, K. and T. Funazukuri, *Depolymerization of poly (ethylene terephthalate) in dilute aqueous ammonia solution under hydrothermal conditions*. Journal of Chemical Technology & Biotechnology: International Research in Process, Environmental & Clean Technology, 2008. **83**(10): p. 1381-1386.
64. Kao, C.Y., W.H. Cheng, and B.Z. Wan, *Investigation of alkaline hydrolysis of polyethylene terephthalate by differential scanning calorimetry and thermogravimetric analysis*. Journal of applied polymer science, 1998. **70**(10): p. 1939-1945.

65. *Tube Fitting Performance Product Test Reports*. 2018 [cited 2020 April 21, 2020];
Available from: <https://www.swagelok.com/downloads/WebCatalogs/en/MS-06-108.PDF>.
66. *Thermophysical Properties of Fluid Systems*. 2018 [cited 2020 April 21, 2020];
Available from: <https://webbook.nist.gov/chemistry/fluid/>.

Appendix

A Parameters of Tube Hydrolysis Reactor Design

Table 2 Parameters for the design, safety and construction of tube hydrolysis reactors adapted from "Tube Fitting Performance Product Test Reports," 2018 [65].

Tube information	
Tube O.D. (in.)	Wall Thickness (in.)
0.5000	0.0650
Area of tube (in. ²)	Area of tube (in. ²)
0.1074	0.6933
Amounts of Feedstocks	
Water (ml)	PET Solid (g)
4.0	0.3
Water Density	
Temperature (K)	Density(g/ml)
473.15	0.86
646.16	0.40
Reactor Configurations	
Initial volume (ml)	4.50
Final volume (ml)	11.79
Length at 372°C (cm)	17.01

Table 3 Tube pressure ratings (a) and steam table data (b) for reactor design.

Table 3 (a) Tube pressure ratings adapted from "Tube Fitting Performance Product Test Reports," 2018 [65].

Temperature (°C)	Max Pressure (psi)	Adjustment Parameter	Adjusted Pressure (psi)
204	5100	0.96	4896
315	5100	0.85	4335
426	5100	0.79	4029

Table 3 (b) Steam table data [66].

Temperature (°C)	Pressure (bar)	Pressure (psi)
201.4	16	232.064
250.3	40	580.16
300.1	88	1276.352
349.8	165	2393.16

B Recent calibration for ethylene glycol (EG)

Table 4 Raw data of ethylene glycol standards

Sample Name	Weight percentage (%)	Area of characteristic peak
EG1	0.041467	15212
EG2	0.022608	8789
EG3	0.017056	5929
EG4	0.006595	2325
EG5	0.002415	1414

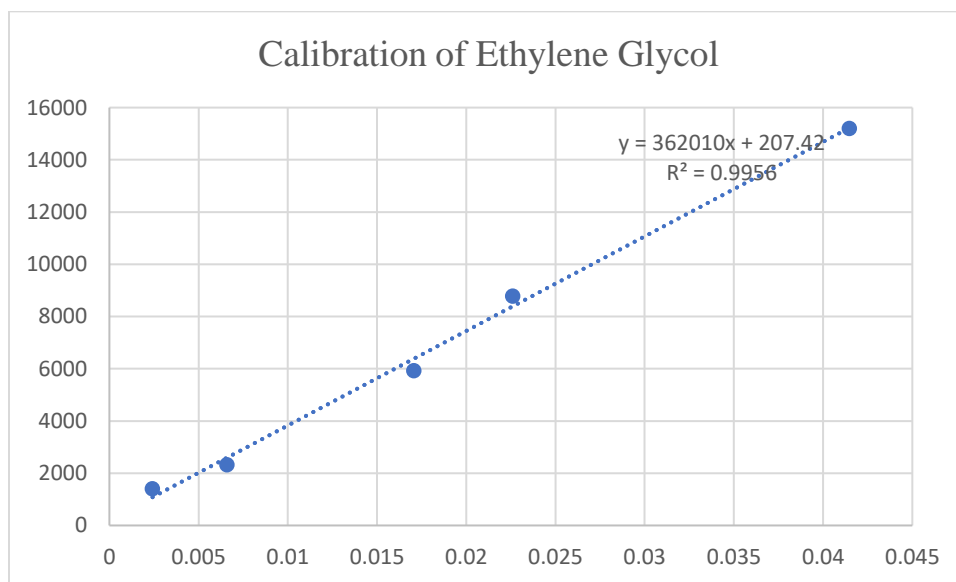


Figure 33 Calibration of Ethylene Glycol.

C Recent calibration for terephthalic acid (TPA)

Table 5 Raw data of terephthalic acid standards

Sample Name	Weight percentage (%)	Abs values
TPA1	0.056391	1.335
TPA2	0.047662	1.257
TPA3	0.041899	1.192
TPA4	0.029881	0.943
TPA5	0.024229	0.801
TPA6	0.019252	0.689
TPA7	0.015946	0.582
TPA8	0.013667	0.472
TPA9	0.009892	0.335

Figure 34 (a) Calibration of TPA (Abs>1.0).

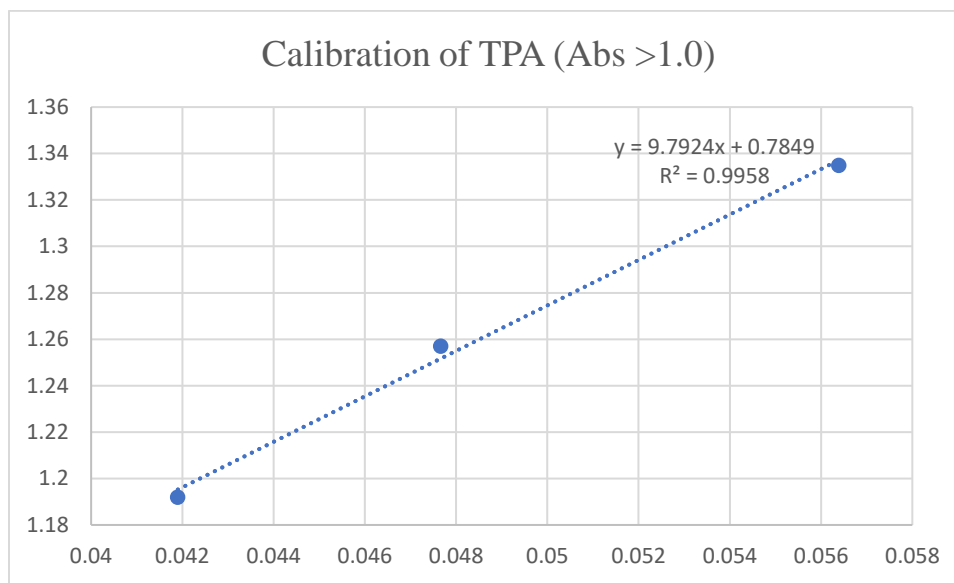


Figure 34 (b) Calibration of TPA ($0.6 < \text{Abs} < 1.0$).

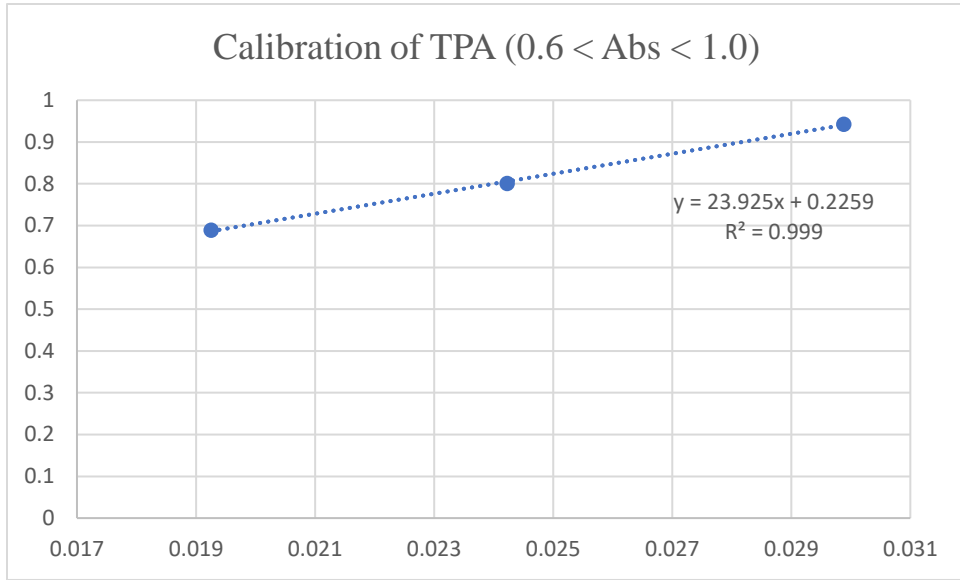


Figure 34 (c) Calibration of TPA (0.3 < Abs < 0.6).

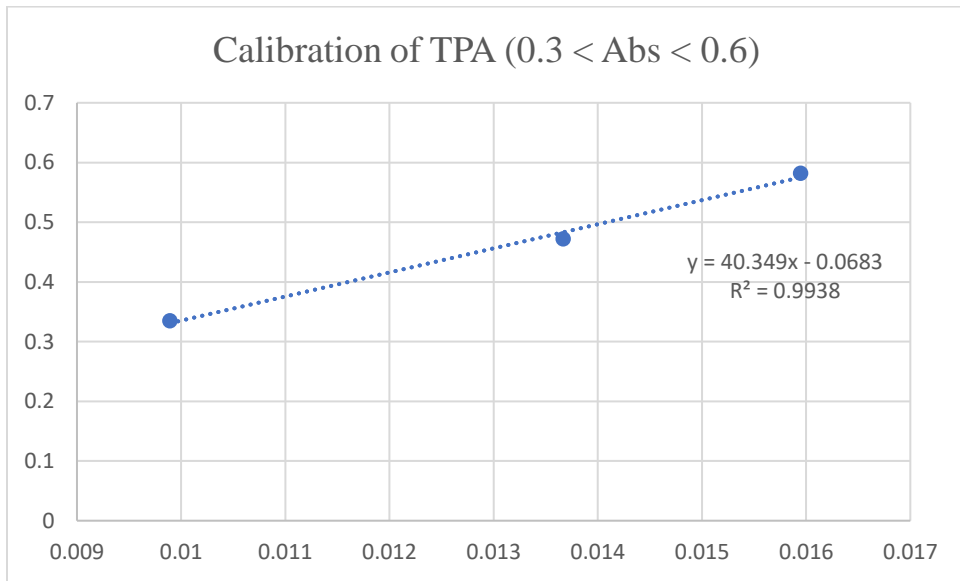


Figure 34 Calibrations of TPA: (a) Calibration of TPA (Abs>1.0), (b) Calibration of TPA (0.6 < Abs < 1.0), (c) Calibration of TPA (0.3 < Abs < 0.6).

D Raw data of PET conversion rates and yields of products

Table 6 Raw data of PET conversion rate based on weight percentage (BM – ball-milled PET samples; FR – fresh PET samples; PH – photoaged PET samples; 1hr – 1 - hour retention time; 2hr – 2 - hour retention time).

Samples Name	Samples (g)	Empty vial (g)	Dried products (g)	Unreacted PET (g)	Conversion Rate (%)
BMA(1hr)	0.3046	13.2339	13.4858	0.2519	17.30
BMB(1hr)	0.3427	13.3371	13.6083	0.2712	20.86
BMC(1hr)	0.3131	13.2899	13.5628	0.2729	12.83
FRA(1hr)	0.3173	13.2733	13.5459	0.2726	14.08
FRB(1hr)	0.3324	13.3103	13.5647	0.2544	23.46
FRC(1hr)	0.3102	13.1818	13.4528	0.2710	12.64
PHA(1hr)	0.3036	13.6714	13.9124	0.2410	20.62
PHB(1hr)	0.3076	13.5876	13.8534	0.2658	13.59
FRI(2hr)	0.3110	13.5464	13.5709	0.0245	92.12
FRII(2hr)	0.3184	13.6433	13.6816	0.0383	87.97
BMI(2hr)	0.3169	13.6319	13.6913	0.0594	81.26
BMII(2hr)	0.3215	13.6792	13.7141	0.0349	89.14

Table 7 Raw data of TPA yield based on weight percentage (BM – ball-milled PET samples; FR – fresh PET samples; PH – photoaged PET samples; 1hr – 1 - hour retention time; 2hr – 2 - hour retention time).

Samples Name	TPA solution (g)	Abs	Wt (%)	TPA produced (g)	TPA (100% depolymerized) (g)	TPA Yield (%)
BMA(1hr)	29.6689	0.985	0.001515124	0.0450	0.2632	17.07
BMB(1hr)	34.8577	0.399	0.000773836	0.0270	0.2962	9.11
BMC(1hr)	44.3302	0.606	0.000571361	0.0253	0.2706	9.36
FRA(1hr)	33.8701	0.712	0.000624406	0.0211	0.2742	7.71
FRB(1hr)	36.4330	0.786	0.000943405	0.0344	0.2873	11.96
FRC(1hr)	42.6714	0.816	0.001105492	0.0472	0.2681	17.59
PHA(1hr)	32.4608	0.779	0.000842688	0.0274	0.2624	10.42
PHB(1hr)	34.4173	0.688	0.000766775	0.0264	0.2658	9.92
FRI(2hr)	30.7350	1.052	0.004508361	0.1026	0.1605	51.00
FRII(2hr)	30.4120	0.505	0.00306312	0.1371	0.2688	39.83
BMI(2hr)	35.7882	0.846	0.004427748	0.1096	0.2752	42.99
BMII(2hr)	26.5936	0.962	0.002767455	0.1177	0.2739	39.03

Table 8 Raw data of TPA yield based on weight percentage (BM – ball-milled PET samples; FR – fresh PET samples; PH – photoaged PET samples; 1hr – 1 - hour retention time; 2hr – 2 - hour retention time).

Samples Name	TPA solution (g)	Abs	Wt (%)	TPA produced (g)	TPA (100% depolymerized) (g)	TPA Yield (%)
BMA(1hr)	25.659	1715	0.004164	0.001069	0.098369	1.086258
BMB(1hr)	29.211	1410	0.003322	0.000970	0.110673	0.876779
BMC(1hr)	20.411	594	0.001068	0.000218	0.101114	0.215562
FRA(1hr)	26.469	959	0.002076	0.000550	0.102470	0.536277
FRB(1hr)	34.267	1104	0.002477	0.000849	0.107347	0.790595
FRC(1hr)	21.482	1292	0.002996	0.000644	0.100177	0.642459
PHA(1hr)	33.263	906	0.001930	0.000642	0.098046	0.654681
PHB(1hr)	25.981	1718	0.004173	0.001084	0.099338	1.091368
FRI(2hr)	21.448	937	0.002015	0.000432	0.060003	11.37221
FRII(2hr)	39.794	10598	0.028702	0.011422	0.100436	8.959681
BMI(2hr)	39.848	8577	0.023120	0.009213	0.102826	5.774204
BMII(2hr)	32.327	6825	0.018280	0.005909	0.102341	12.26969

Table 9 Raw data of PET conversion rate, yield of TPA and yield of EG.

	PET	TPA	ER
BM	17.00149	11.84630	0.72619
FR	16.73011	12.42258	0.65644
PH	17.10416	10.17482	0.82214
FR	90.04665	45.41844	10.16594
BM	87.62346	41.01021	9.02194

E XRD peak fitting

Table 10 Raw data of XRD peak fitting.

Ball-milling time	Total area	Amorphous area	Total area	Amorphous area	Degree of crystallinity (%)
0	20304	12530	1	0.62	19.7
35	26007	18542	1	0.71	14.8
70	21130	16570	1	0.78	11.1

F FT-IR spectra of recovered TPA

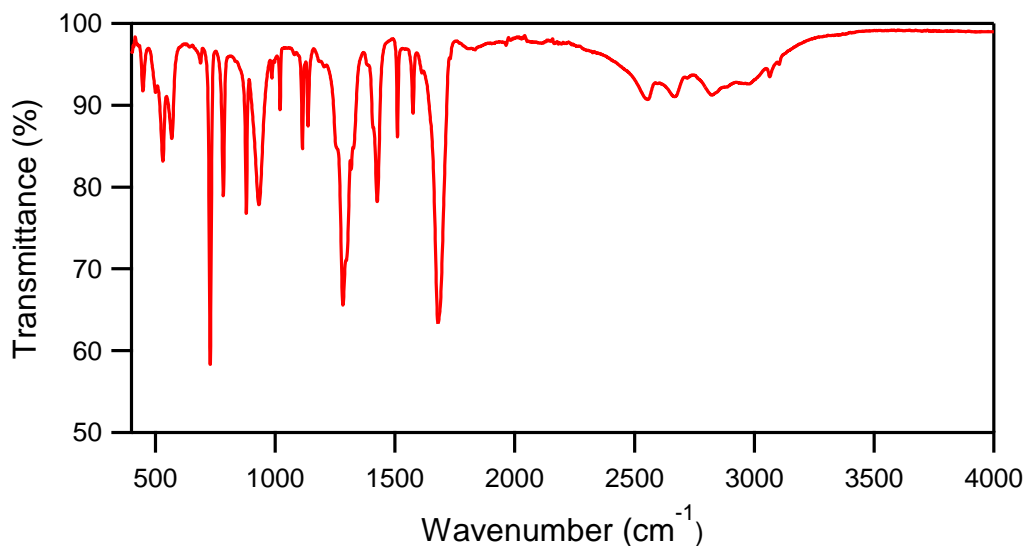


Figure 35 FT-IR spectrum of recovered TPA from hydrolyzed solid products and standard TPA (Fresh PET, 1 hour).

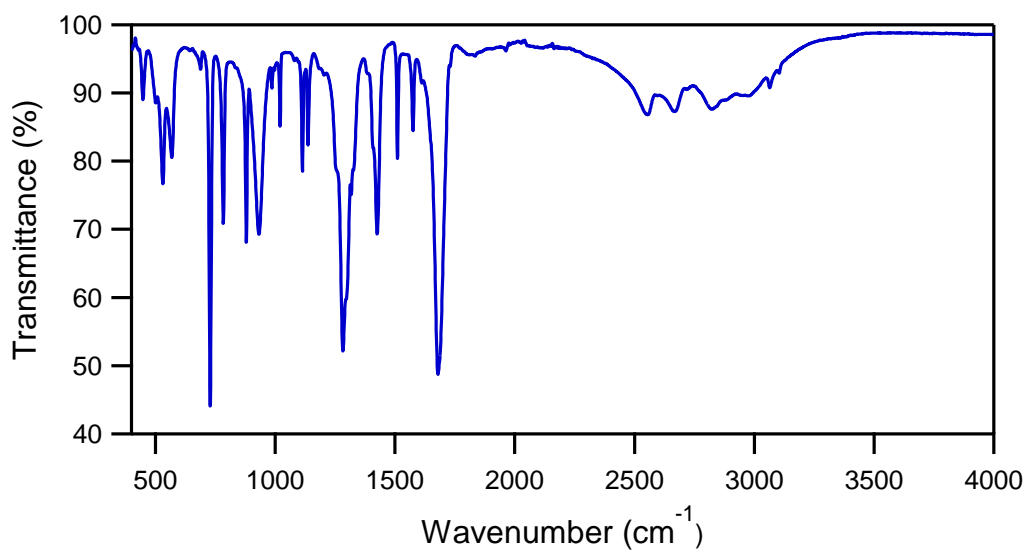


Figure 36 FT-IR spectrum of recovered TPA from hydrolyzed solid products and standard TPA (Fresh PET, 2 hours).

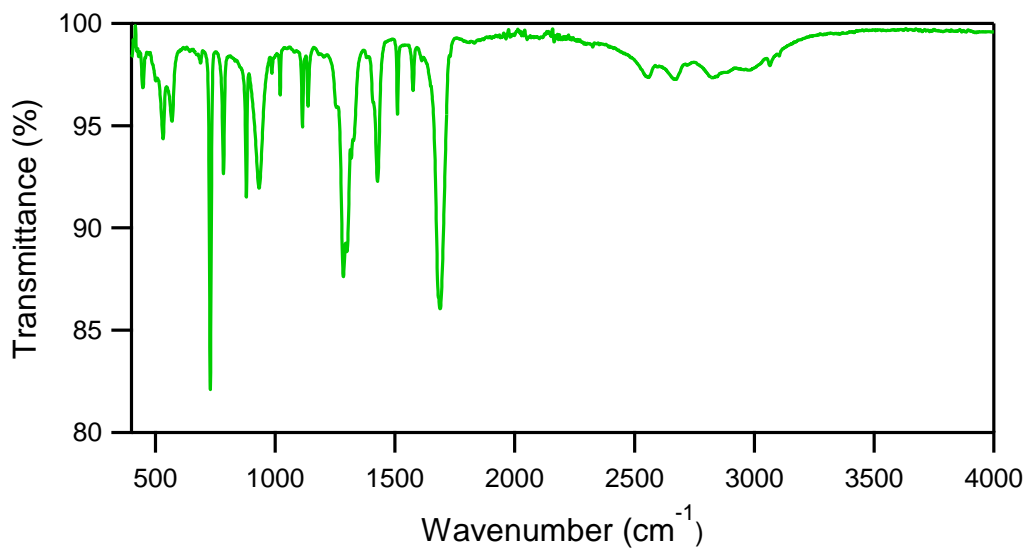


Figure 37 FT-IR spectrum of recovered TPA from hydrolyzed solid products and standard TPA (Ball-milled PET, 1 hour).

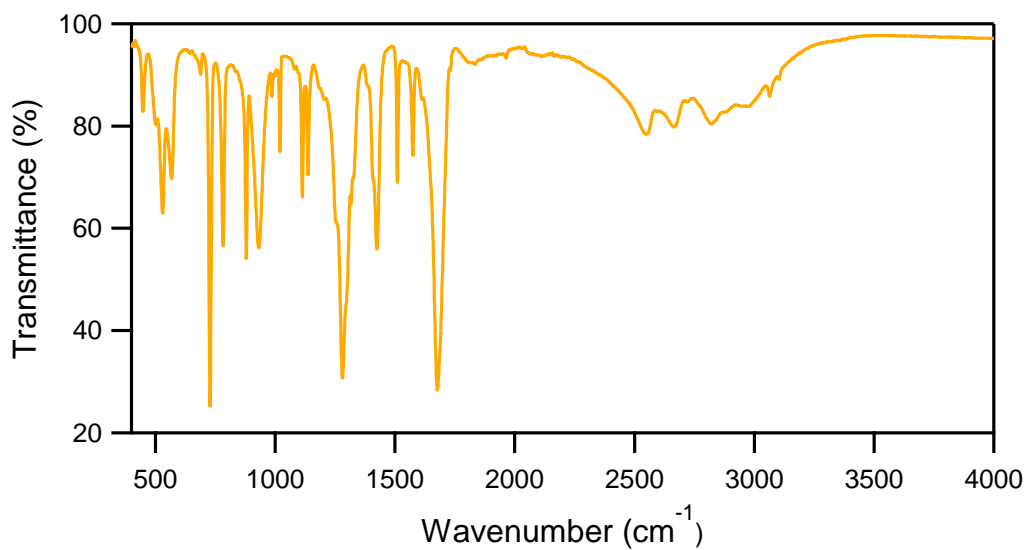


Figure 38 FT-IR spectra of recovered TPA from hydrolyzed solid products and standard TPA (Ball-milled PET, 2 hours).